An *In Vitro* Platform to Spatiotemporally Control Multiple Bioactive Peptides Using Reversible DNA Handles

by

Fallon M. Fumasi

A Dissertation Presented in Partial Fulfillment
of the Requirements for the Degree
Doctor of Philosophy

Approved October 2021 by the
Graduate Supervisory Committee:

Julianne L. Holloway, Chair
Nicholas Stephanopoulos
Matthew D. Green
Sarah E. Stabenfeldt
Abhinav Acharya

ARIZONA STATE UNIVERSITY

December 2021

ABSTRACT

The natural healing process for bone has multiple signaling cascades where several soluble factors are expressed at specific times to encourage regeneration. Human mesenchymal stromal cells (hMSCs) have three stages of osteogenic differentiation: an increase in cell number (day 1-4), early cell differentiation showing alkaline phosphatase (ALP) expression (day 5-14), and deposition of calcium and phosphate (day 14-28). The first two stages are of particular interest since cell adhesion peptides have been shown to have biological significance during these early stages of bone regeneration. However, far less is known about the temporal dependence of these signals.

To mimic these complex systems, developing dynamic biomaterials has become a popular research area over the past decade. Advances in chemistry, materials science, and manufacturing have enabled the development of complex biomaterials that can mimic dynamic cues in the extracellular matrix. One specific area of interest is spatiotemporal control of multiple biomolecules; however, this has generally required diverse chemical approaches making the process difficult and impractical. To circumvent these issues, I developed a novel method that combines a photoresponsive hydrogel with single-stranded DNA to spatiotemporally control multiple biomolecules using a single conjugation scheme.

Here, I describe a detailed protocol to manufacture a fully reversible, spatiotemporal platform using DNA handles. Norbornene-modified hyaluronic acid hydrogels were used to spatially control biomolecule presentation while single-stranded DNA was used to temporally control biomolecule presentation via toehold-mediated

strand displacement. This platform was used to orthogonally control the presentation of multiple biomolecules with simple and complex spatial patterning, as well as control the cell morphology of hMSCs by tuning the presentation of the cell adhesion peptide RGDS.

Then, this system was applied to study the temporal presentation of cell adhesion peptides and their effect on early osteogenic differentiation of hMSCs *in vitro*. The peptides used were RGDS, HAVDI, and OGP. OGP alone expressed higher ALP when presented from day 7-14 than day 0-7 or 0-14. When RGDS, HAVDI, and OGP were combined, there was an increase in ALP activity when HAVDI was presented from day 0-3 indicating that HAVDI plays an important role at earlier time points during osteogenic differentiation.

Dedicated to…
My Mom and Dad

ACKNOWLEDGMENTS

I would like to sincerely thank everyone that has helped, supported, and pushed me throughout my life. You have all had an impact on the person I am today and for that I am grateful. I am especially grateful for the continued love and support of my parents (Dean and Michele) and my brothers (Briley and Theron). You have always been there for me during my greatest and weakest moments and have always encouraged me to pursue what I want in life.

I would like to thank my advisor Dr. Julianne Holloway for her guidance and mentorship through my PhD and providing me with opportunities to prepare me for the next chapter in my life. Additionally, I would like to thank Dr. Nicholas Stephanopoulos who acted as my unofficial co-advisor throughout my PhD. His support and mentoring have shown me how to remain positive, upbeat, and excited about the work I have and will be doing in the future.

Lastly, none of this would have been possible without the support of my friends. They have provided me with a support network both in and out of the lab and have made this a fun and memorable experience. Thank you to Tara MacCulloch, Julio Bernal, Grace Schwarz, Gregory Jensen, and Kassondra Hickey for being great lab mates and friends. You always made the lab a fun and inviting place and have provided numerous insights and discussions to further my knowledge and mentorship. Thank you to Nora Martin for our weekly girls' nights and being a supportive friend. And a special thank you to Kenneth Manning and R. Kevin Tindell whose friendship has been unwavering, and I could not have asked for better friends to go through this process with here at ASU.

I would like to thank Arizona State University for providing start-up funding, the Advanced Light Microscopy Core for use of their instruments, the Magnetic Resonance Research Center for use of their NMR instrument, and Dr. Sarah Stabenfeldt for use of her fluorescent microscope. This work was supported through the National Institutes of Health funding R21AR074069.

TABLE OF CONTENTS

Page

CHAPTER Page

LIST OF TABLES

LIST OF FIGURES

CHAPTER 1

INTRODUCTION AND MOTIVATIONS

(Adapted from: F.M. Fumasi, N. Stephanopoulos, and J.L. Holloway, "Reversible control of biomaterial properties for dynamically tuning cell behavior," J. Appl. Polym. Sci., 2020, 137: e49058)[1]

1.1 The Healing Cascade

The human body is constantly influenced by biochemical and biophysical cascades that affect development, homeostasis, regeneration, wound healing, and disease progression.[2–4] These signaling cascades are strictly regulated, highly complex, and dynamic—spatially and temporally—influencing all tissue types. Specifically, during the healing process, multiple soluble factors are expressed at specific times to sequentially encourage inflammation, cell migration, proliferation, differentiation, and new tissue formation.[5,6] For example, bone has four stages of fracture repair with three main groups of soluble factors—inflammatory cytokines, morphogens, and angiogenic factors—that play a key role in regulating these processes.[5,7–9] During the initial injury phase, there is a large increase mainly in inflammatory cytokines to help control inflammation and increase cell death to encourage new cell growth to the injured site. Next, there is a surge primarily in morphogens during the endochondral and primary bone formation stages to aide in periosteal response and cartilage resorption, respectively. Lastly, high levels of predominantly angiogenic factors can be seen during the primary and secondary bone formations stages to provide new vascularization to aide in remodeling bone tissue. The presentation and level of expression of these factors dynamically changes as it progresses through each stage of healing (**Figure 1.1**); however, the vast number and the

spatiotemporal presentations of these biomolecules makes developing new biomaterials capable of replicating these cues challenging.

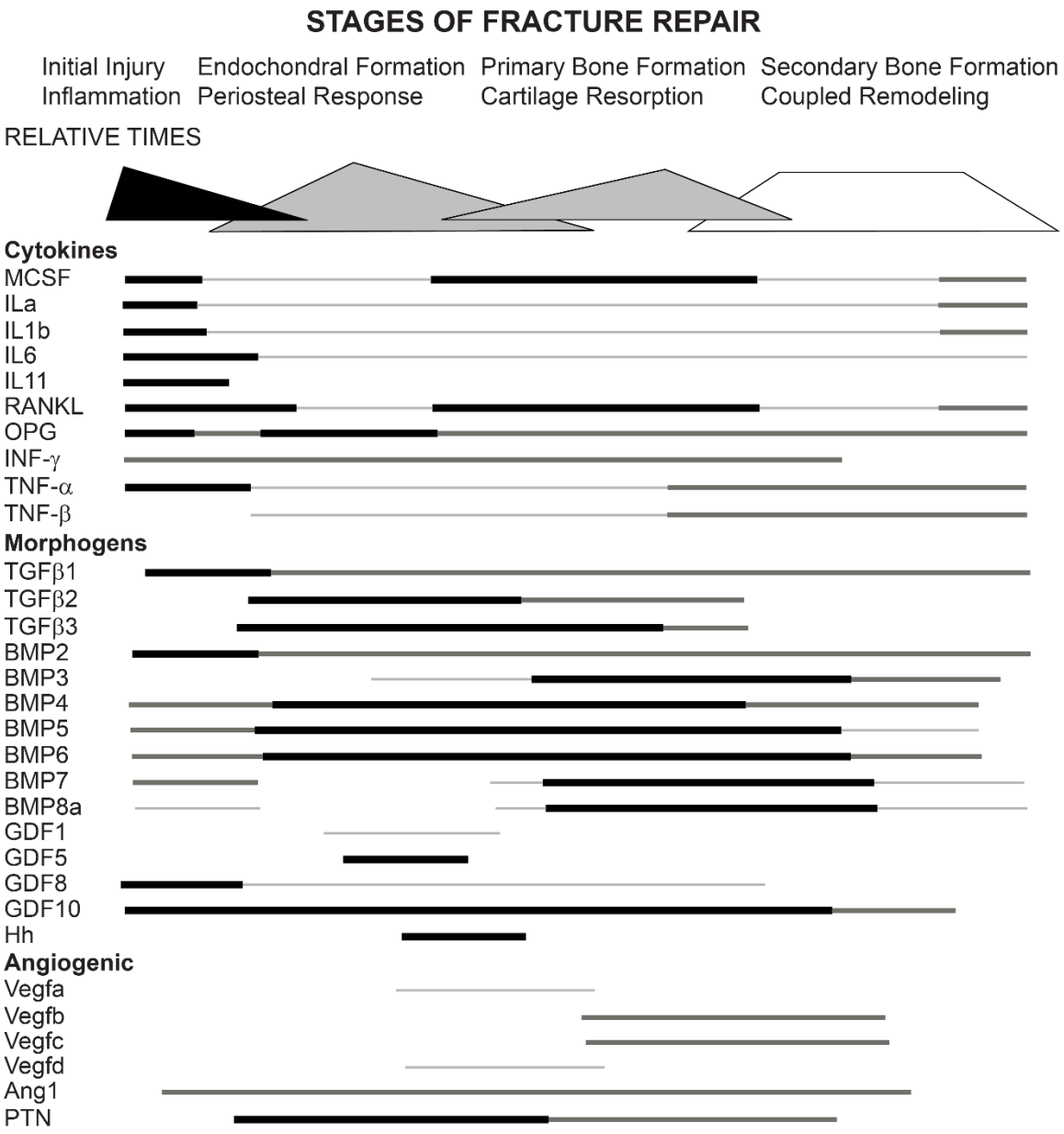

Figure 1.1: Stages of fracture repair and biomolecule presentation. The geometric shapes represent the relative temporal aspects of each stage. The relative levels of mRNA expression of the three main groups of soluble factors are denoted by three line widths and colors (thick = black, medium = dark gray, thin = light gray).[5]

1.2 Biomaterials

Traditional research has focused on the use of static, homogenous biomaterials, where material properties are constant in both space and time.[10,11] Research using these static materials has elucidated the relationship between material signaling cues (e.g. topography, stiffness, and bioactive ligands) and cell behavior (e.g. cell spreading, proliferation, and differentiation).[12–15] However, there have been advances in materials science, chemistry, and manufacturing that have enabled the development of more complex biomaterials that start to mimic the dynamic spatiotemporal signaling cues present during healing and disease progression.

1.2.1 Techniques that Provide Spatial Control

Recent changes in manufacturing have created biomaterials with improved spatial control and hierarchal organization. To achieve spatial resolution for different designs, photopatterning, lithography, electrospinning, microfluidic-based systems, and three-dimensional bioprinting have been used to create chemical changes throughout biomaterials.[16–18] Photopatterning and lithography both work based on the use of a light-triggered source to activate chemical changes such as chemically conjugating biomolecules to the surface[19–21] or exposing caged biomolecules to change the bioactivity of the material at specific locations.[22–24] Electrospinning creates a fibrous mat, where the biomolecules can be controlled to develop gradients using different types of electrospinning setups: coaxial-electrospinning, in-line blending, and air-gap electrospinning.[25–27] Microfluidics have been used to create patterns on modified surfaces by placing the microfluidic device on the biomaterial surface and flowing the

biomolecules of interest through the channels for binding to occur at the modified locations.[28,29] Lastly, by using additive manufacturing through 3D printing, biomolecules can be incorporated into the print solution while multiple extrusion jets can control different print solutions to spatially control biomolecule presentation throughout the entire printed structure.[17,30–32] All of these techniques provide a method to control biomolecules in space; however, others have studied how different chemistries can provide temporal control of biomolecules.

1.2.2 Chemistries that Provide Reversible Temporal Control

Temporal control of biomolecule presentation can be administered via encapsulation and degradation or using covalent or noncovalent chemistries to tether the biomolecule to the platform. However, the use of encapsulated biomaterials is an irreversible system; once the biomolecule is released there is no re-addition of the biomolecule at a later time point. Nevertheless, a few covalent and noncovalent chemistries do allow for reversibility and provide temporal control of biomolecule presentation under physiological conditions. Some examples of covalent chemistries with temporal control are exchange, oxidation-reduction (redox), isomerization, and the combination of addition and cleavage reactions. Auernheimer et al. developed photo-switchable controls using an azobenzene unit that changed conformation when UV or visible light was presented to control RGDS bioactivity.[33] Alternatively, Lamb and Yousaf designed a redox-switchable surface that cycles between a cyclic and linear RGD structure (with cells binding more tightly to the former) using oxyamine-terminated ligands on hydroquinone-terminated self-assembled monolayers.[34]

Two different types of noncovalent chemistries have also been used to control biomolecule presentation: guest-host and DNA hybridization. Boekhoven et al. used guest-host chemistry to modify alginate surfaces with β-cyclodextrin (host) and two different guest molecules for reversibility (naphthyl-RGDS and adamantane-RGES; adamantane is a better guest for cyclodextrin than naphthalene, so the RGDS signal could be replaced by the RGES peptide, effectively switching bioactivity off).[35] Freeman et al. created a molecular system that used peptide-DNA conjugates to add or remove two different bioactive signals on alginate coated surfaces.[36] The authors immobilized single-stranded DNA (ssDNA) handles on the surface before adding a complementary DNA strand modified with the biomolecule of interest. A displacement strand removed the bioactive ligand—via toehold-mediated strand displacement—leaving the initial tethered strand on the surface, so the peptide could be added back in a second cycle. This type of system allows for switching between an "ON" or "OFF" state over multiple cycles and, in principle, could be extended to three or more signals given the vast number of orthogonal (independent) DNA sequences. However, each of the described approaches lacks spatial control over biomolecule cues.

1.2.3 Spatiotemporal Control of Biomolecule Presentation

In recent years, there has been a surge of interest in dynamically controlling the presentation of bioactive signals with spatiotemporal precision. Few groups have been able to develop spatiotemporal platforms. Laser photolithography has been widely used to spatially control biomolecule presentation[37–40] while two different types of photo-click chemistries have been used to add temporal control to these biomaterials.[41–46]

Some groups have used the addition of lysine(allyloxycarbonyl) amino acid[41,42] or a photo-deprotected oxime-ligation[43,44] (addition) in combination with a cleavable o-nitrobenzyl moiety (cleavage) to spatiotemporally control biomolecule presentation. Even though these systems are reversible and can spatially control multiple biomolecules, the use of two conjugation schemes lack simplicity and ease of use. Others have used reversible allyl sulfide (exchange) reactions to improve temporal control by using a single conjugation method.[45,46] This method undergoes addition fragmentation chain transfer which simultaneously provides controlled addition and removal of biomolecules as well as regenerating the reactive functionality. However, the one downfall to this system is that it lacks orthogonality – it cannot be used to temporally control multiple biomolecules independently. When developing a spatiotemporal platform, reversibility (i.e. add and remove the biomolecule over multiple cycles) and orthogonality (i.e. independent control of multiple biomolecules using the same reaction scheme) are especially important since cells depend on many different signals at different time points to promote specific behavior. The development of a dynamic platform that mimics the natural healing cascade would enable a deeper understanding of the cell signaling pathways involved and the role of different biomolecules during healing.

1.3 DNA as a Reversible Handle

Branching off of Freeman et al., DNA provides reversibility, orthogonality, and simplicity. [36] Structural DNA nanotechnology became an emerging field in the early 1980s and has grown significantly over the past 40 years.[47] DNA assembly occurs when hydrogen bonds form between adenine and thymine exclusively and cytosine and guanine

exclusively—otherwise known as Watson-Crick base pairing.[48–52] This exclusive pairing allows for high programmability and specificity when using DNA as a molecular building block to construct self-assembled nanostructures. This also gives DNA the advantage of creating dynamic systems with the most common approach being toehold-mediated strand displacement.[51,53,54] This approach can switch DNA assemblies by incorporating a short, single-stranded overhang or "toehold" (**Figure 1.2, brown**) onto one of the duplex strands. This longer strand can be removed by presenting a complementary displacement strand that binds to the toehold region and breaks the duplex by outcompeting the shorter strand via branch migration (**Figure 1.2**). Since strand displacement is sequence-specific, this mechanism can provide reversibility and orthogonality to a biomaterial by tethering peptides onto the ssDNA with the toehold region to reversibly control the presentation of biomolecular signals.

Due to its structural specificity,[51,55] DNA has been used to create a multitude of complexes—such as prisms,[56] tetrahedrons,[57] box origami,[58] etc.—and has been used to advance biomedical applications. Recently, there has been a large interest in using DNA to develop self-assembled, functional biomaterial scaffolds to interact with cells. For example, research groups have used DNA to create DNA-only hydrogels using different branched DNA building blocks[59,60] or used DNA as a force sensor to report cellular forces.[61–63] Others have used the toehold-mediated strand displacement technique with DNA as a crosslinker to reversibly alter mechanical stiffness[64] or with DNA as a tether to control peptide-DNA presentation.[36] Even though researchers have used DNA to provide reversibility and orthogonality over temporal biomolecule presentation, there has been a lack of spatial control which could be used to explore how

multiple bioactive signals can synergistically or antagonistically affect cell behavior on a single platform. In order to accomplish this, it is necessary to have a vast knowledge of different bioconjugation strategies, not only for creating these peptide-DNA conjugates, but for spatially tethering DNA to these biomaterial surfaces.[65]

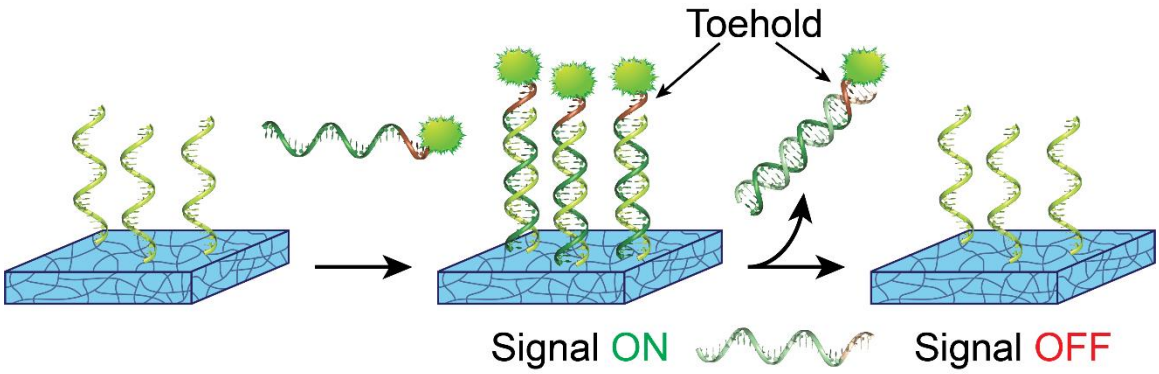

Figure 1.2: Schematic of toehold-mediated strand displacement. ssDNA is tethered to the biomaterial (left). A complementary biomolecule-DNA strand with a toehold region (brown) is introduced and forms a duplex with the tethered strand turning the signal "ON" (middle). A fully complementary displacement DNA strand binds to the toehold region and outcompetes the tethered strand to remove the biomolecule-DNA strand turning the signal "OFF" (right).

1.4 Approach

Most dynamic systems that control ligand presentation rely on either UV-switchable groups (e.g. azobenzenes), which are potentially harmful to cell viability, or cleavable moieties (e.g. nitrobenzyl esters), which are irreversible. Another challenge is orthogonally controlling multiple ligands which is synthetically challenging and impractical for more complex systems. Currently, there is no *in vitro* platform that can reversibly control three (or more) signals over multiple cycles in both space and time using a single bioconjugation scheme. Due to the benefits of DNA mentioned previously, I propose using DNA as a reversible linker—combined with a modified hyaluronic acid

(HA) hydrogel—to develop an *in vitro* DNA-based hydrogel platform that can independently and reversibly control the spatiotemporal presentation of multiple biomolecules. The development of this platform would better mimic the natural healing process thereby facilitating a deeper understanding of the synergistic or antagonistic effects of multiple biomolecular signals on cell behavior. To demonstrate the utility of such a system, this platform will be used to investigate the temporal role of various biomolecules on osteogenesis with the central hypothesis being that interactions between multiple bioactive ligands (e.g. cell-cell, cell-matrix, and osteogenic growth factor) can dramatically enhance or otherwise influence osteogenic differentiation. Specifically, it is expected that cell-cell interactions will play a larger role at earlier time points to promote differentiation[66–68] while cell-matrix interactions are important at later time points to enhance matrix mineralization.[69–72] The following objectives are:

<u>OBJECTIVE 1</u>: Develop a platform for spatially and temporally controlling biomolecule immobilization using reversible DNA hybridization. A model HA-based platform will be developed using fluorophore-labeled DNA as a proof of concept to control fluorescent signaling both spatially and temporally. First, single-stranded DNA (ssDNA) will be tethered to the hydrogel surface via photopatterning to impart spatial control. Then, a fluorophore-labeled complementary strand will be presented to the surface to undergo hybridization. To allow for selective removal of the signal, toehold-mediated strand displacement will be utilized.[73] Implementing a toehold region will provide reversible temporal control to the system. Finally, by using DNA as a common linker, changing the DNA sequence allows for orthogonal control of multiple biomolecules.

<u>OBJECTIVE 2</u>: Evaluate how the temporal presentation of RGDS, HAVDI, and OGP affects osteogenic differentiation. The platform developed in **Objective 1** will be used to study how the temporal presentation of cell adhesion molecules and the osteogenic growth peptide affect osteogenic differentiation. The cell adhesion molecules RGDS and HAVDI will be used to mimic cell-matrix and cell-cell interactions, respectively. The growth factor osteogenic growth peptide (OGP) will be used to facilitate osteoinduction. First, RGDS, HAVDI and OGP peptides will be synthesized in house and conjugated to ssDNA strands. Then, OGP will be studied independently to evaluate how temporal changes to OGP affects osteogenic differentiation. Lastly, a combination of RGDS, HAVDI, and OGP with be temporally presented at various time points to understand the role of cell-cell and cell-matrix interactions on early osteogenic differentiation.

CHAPTER 2

SAFETY

Before evaluating the experiments conducted in relation to this thesis, it is imperative that the safety aspects of this work be highlighted to mitigate risks and promote a safe working environment. All Arizona State University environmental health and safety (EH&S) protocols as well as Holloway Laboratory safety protocols were followed throughout the duration of this work. This work requires potential exposure to both biological and chemical hazards. In the event of a spill, any biological spill was cleaned using disinfectant (freshly prepared 10% bleach) allowing for a contact time of at least 20 minutes. Decontaminated waste material was placed into a biological waste container lined with a biohazard bag. Clean-up equipment will be decontaminated using one of the following methods: soaked with 10% bleach or sterilized using an autoclave. Chemical waste was stored in appropriate waste containers (i.e. aqueous, organics, and acids were stored in separate containers) in the fume hood. All waste was collected and properly disposed of by ASU EH&S.

The general personal protective equipment (PPE; i.e. safety glasses, laboratory coat, gloves, long pants, and close-toed shoes) were used at all times when working in the lab while additional PPE was donned for specialized tasks. When working with hMSCs, samples were handled in a BSL-2 rated biological safety cabinet (BSC). The BSC is certified on an annual basis to verify that it is operating within normal ranges. hMSCs are stored long term in a cryogenic tank under liquid nitrogen, so cryogenic gloves were worn, in addition to general PPE, when working with the vessel. Multiple chemicals used

for fixation and staining cells are known mutagens and/or carcinogens and were handled exclusively in the fume hood.

To protect skin and eyes from dangerous exposure, UV safety glasses were worn, in addition to general PPE, when using the UV light to cure and photopattern hydrogels. This work required using high concentrations of sodium hydroxide as well as dichloromethane and (3-mercaptopropyl)trimethoxysilane (MPTS) and was performed in the fume hood to avoid exposure. Additionally, a ventilated oven was used to prevent exposure to MPTS fumes during sample processing. Temperature resistant gloves were worn, in addition to generally PPE, when using the autoclave or handling samples from the oven when at high temperatures. Lastly, NorHA was synthesized under inert conditions, so sharps (e.g. cannula, needles) were used to transfer solutions from vessel to vessel. Secondary needles were inserted as pressure relief valves and a bubbler was hooked up in-line with the system to monitor the gas flowrate and to mitigate the chances of over pressurizing glass vessels. This process was also completed in the fume hood with the sash down for additional protection.

CHAPTER 3

DEVELOPMENT OF A REVERSIBLE HYALURONIC ACID-BASED PLATFORM WITH SPATIOTEMPORAL CONTROL OF DNA-LINKED LIGANDS

3.1 Introduction

The biochemical and biophysical cues within all tissues are strictly regulated in both space and time. In particular, biomolecular signaling cascades are highly complex and dynamic—both spatially and temporally—and influence development, homeostasis, regeneration, wound healing, and disease progression.[2–4] During the healing process, multiple soluble factors are expressed at specific times to sequentially encourage inflammation, cell migration, proliferation, differentiation, and new tissue formation.[5,6] Developing biomaterials that can mimic this dynamic signal presentation is an ongoing challenge and only a handful of groups have developed platforms that reversibly control biomolecule presentation. However, most use covalent chemistries that require different reactions and/or wavelengths to achieve reversibility.[41–46] Due to this issue, there is typically a lack of orthogonal control over multiple biomolecules in both space and time. Currently, there are no systems that allow for complete reversibility and spatial control of multiple biomolecules using a single reaction scheme.

One potential solution is to use DNA as a programmable linker for biomolecule display, due to the high programmability and specificity of oligonucleotide base pairing. DNA has, for example, been used as a linker to reversibly change the stiffness of a hydrogel[74,75] or to control the presentation of peptides and proteins.[36] However, DNA has not been combined with a spatially controlled platform to enable both spatial and

temporal control over biomolecule presentation. In this chapter, I provide a detailed outline to fabricate a fully reversible, spatiotemporally controlled platform that combines programmable DNA handles with a photoresponsive hyaluronic acid scaffold. These DNA handles can be used to control the independent presentation of multiple biomolecules (e.g. peptides, proteins, polymers) by tethering to a complementary DNA handle with reversibility enabled using toehold-mediated strand displacement. The development of this type of *in vitro* platform would allow users to better understand cell biology by studying how multiple biomolecules affect cell behavior in both space and time. This level of understanding could inspire new developments in drug delivery, regenerative medicine, tissue engineering, and more.

3.2 Materials

3.2.1 Hyaluronic Acid Tert-Butyl Ammonium Salt (HA-TBA) Synthesis

Reagents:

- ✓ Sodium hyaluronate (Na-HA), 66-99 kDa (Lifecore Biomedical, USA, Cat#: HA60K-5)
- ✓ AmberChrom® 50WX4 ion exchange resin, 50-100 mesh (previously Dowex®, Millipore Sigma, USA, Cat#: 428663-100G)
- ✓ Tetrabutylammonium hydroxide (TBA-OH) (Millipore Sigma, USA, Cat#: 86880-100ML)
- ✓ Deionized (DI) water
- ✓ Deuterium oxide (D_2O) (Fisher Scientific, USA, Cat#: AC426931000)

Equipment:

- ✓ 500 mL round bottom flask (RBF) (Fisher Scientific, USA, Cat#: 10-068-1D)
- ✓ Magnetic stir plate (Fisher Scientific, USA, Cat#: 07-250-140)
- ✓ Glass filtering flask, 500 mL with side arm (Fisher Scientific, USA, Cat#: K617500-0005)
- ✓ Buchner funnel (Fisher Scientific, USA, Cat#: 10-362D)
- ✓ Filter paper, grade 2 (Fisher Scientific, USA, Cat#: 09-810D)
- ✓ pH meter (Fisher Scientific, USA, Cat#: 13-303-200)
- ✓ Lyophilizer (VWR, USA, Cat#: 76000-478)
- ✓ ^{1}H nuclear magnetic resonance (^{1}H NMR), (500 MHz, Bruker, USA)
- ✓ NMR tubes and caps (VWR, USA, Cat#: 82005-334)

3.2.2 Norbornene-Modified Hyaluronic Acid (NorHA) Synthesis

Reagents:

- ✓ HA-TBA created in *Step 3.3.1* in the Procedure section
- ✓ 5-norbornene-2-methylamine (nor-amine) (Fisher Scientific, USA, Cat#: N09075G)
- ✓ Benzotriazole-1-yl-oxy-tris-(dimethylamino)-phosphonium hexafluorophosphate (BOP) (Millipore Sigma, USA, Cat#: 8510040025)
- ✓ Anhydrous dimethyl sulfoxide (DMSO) (Millipore Sigma, USA, Cat#: 276855-100ML)
- ✓ Acetone (Millipore Sigma, USA, Cat#: 320110-4L)
- ✓ Sodium hydroxide (NaOH), (VWR, USA, Cat#: MK770806)

- ✓ Sodium chloride (NaCl), (Millipore Sigma, USA, Cat#: S9888-1KG)
- ✓ Deionized (DI) water
- ✓ Deuterium oxide (D_2O) (Fisher Scientific, USA, Cat#: AC426931000)

Equipment:

- ✓ 250 mL round bottom flask (RBF) (Fisher Scientific, USA, Cat#: 10-068-1C)
- ✓ 100 mL round bottom flask (RBF) (Fisher Scientific, USA, Cat#: 10-068-1B)
- ✓ Magnetic stir plate (Fisher Scientific, USA, Cat#: 07-250-140)
- ✓ Cannula (VWR, USA, Cat#: 80060-152)
- ✓ 22 ga 1.5” needles (Fisher Scientific, USA, Cat#: 14-815-525)
- ✓ Dialysis tubing (6000-8000 MWCO), (Fisher Scientific, USA, Cat#: 08-670D)
- ✓ 40 µm cell strainer (Fisher Scientific, USA, Cat#: 22-363-547)
- ✓ pH meter (Fisher Scientific, USA, Cat#: 13-303-200)
- ✓ Lyophilizer (VWR, USA, Cat#: 76000-478)
- ✓ ^{1}H nuclear magnetic resonance (^{1}H NMR) (500 MHz, Bruker, USA)
- ✓ NMR tubes and caps (VWR, USA, Cat#: 82005-334)

3.2.3 Peptide Synthesis and Purification

Reagents:

- ✓ Standard Fmoc-protected amino acids: Fmoc-Gly-OH, Fmoc-Tyr(*t*Bu)-OH, Fmoc-Arg(Pbf)-OH, Fmoc-Asp(O*t*Bu)-OH, Fmoc-Ser(*t*Bu)-OH, Fmoc- Pro-OH, Fmoc-AzK-OH (Novabiochem®, USA)
- ✓ N,N-dimethylformamide (DMF) (Oakwood Chemical, USA, Cat#: 046776)
- ✓ Piperidine (Millipore Sigma, USA, Cat#: 104094)

- ✓ N,N-diisopropylcarbodiimide (DIC) (Millipore Sigma, USA, Cat#: 8036490025)
- ✓ N,N-diisopropylethylamine (DIEA) (Millipore Sigma, USA, Cat#: D125806)
- ✓ Ethyl cyano(hydroxyimino)acetate (Oxyma) (Chem-Impex Int'l Inc., USA, Cat#: 26426)
- ✓ Rink Amide AM resin (100-200 mesh) (Millipore Sigma, USA, Cat#: 8.55130)
- ✓ Trifluoroacetic acid (TFA) (Millipore Sigma, USA, Cat#: 108262)
- ✓ Triisopropylsilane (TIPS) (Oakwood Chemical, USA, Cat#: S17975)
- ✓ 2,2-(ethylenedioxy)diethanethiol (DODT) (Millipore Sigma, USA, Cat#: 465178)
- ✓ Diethyl ether (Et_2O) (Oakwood Chemical, USA, Cat#: 101608)
- ✓ Acetonitrile (ACN), HPLC grade (Oakwood Chemical, USA, Cat#: 099891)
- ✓ α-Cyano-4-hydroxycinnamic acid (CHCA) (Spectrum Chemical Manufacturing Corp., USA, Cat#: C3120)
- ✓ Deionized (DI) water

Equipment:

- ✓ Peptide synthesizer (CEM, Liberty Blue, USA)
- ✓ Microcentrifuge (Hettich, Mikro 200, Germany)
- ✓ Centrifuge (Thermo Scientific, Sorvall Legend XTR, USA)
- ✓ Vortex mixer (VWR, USA, Cat#: 10153-688)
- ✓ Peptide synthesis cleavage vessel (Chemglass, USA, polytetrafluoroethylene (PFTE) 100 mL, Medium Frit, Cat#: 80071-354)
- ✓ Wrist action shaker (Burrell, USA, Cat#: 14-400-122)
- ✓ Polyvinylidene fluoride (PVDF) syringe microporous filters (Whatman, USA, UNIFLO, 25mm x 0.22µm, Cat#: 09-928-030)

- ✓ Semipreparative high performance liquid chromatography (HPLC) system (Water, LC Prep 150, USA)
- ✓ UV/Vis Nanodrop detector (Thermo Scientific, Nanodrop One, USA)
- ✓ Matrix-assisted laser desorption ionization time of flight mass spectrometer (MALDI TOF MS) (Bruker, Microflex LRF MALDI, USA)

3.2.4 Peptide-DNA Conjugation and Purification

Reagents:

- ✓ 5'-amine-modified oligonucleotides (1 µmole scale, Integrated DNA Technologies, Inc, USA)
- ✓ Sodium chloride (NaCl) (Fisher Scientific, USA, Cat#: BP358-10)
- ✓ Potassium chloride (KCl) (Millipore Sigma, USA, Cat#: P3911)
- ✓ Sodium phosphate dibasic (Na_2HPO4) (VWR, USA, Cat#: 0404)
- ✓ Potassium phosphate monobasic (KH_2PO_4) (VWR, USA, Cat#: 0781)
- ✓ Sodium hydroxide (NaOH) (Fisher Scientific, USA, Cat#: S320)
- ✓ Dibenzocyclooctyne-sulfo-N-hydroxysuccinimidyl ester (DBCO-Sulfo-NHS) (Millipore Sigma, USA, Cat#: 762040)
- ✓ Ultrapure water (Millipore Sigma, USA, Cat#: Q-POD)
- ✓ 1 M Triethylammonium acetate (Millipore Sigma, USA, Cat#: 625718)
- ✓ Methanol (MeOH) (Honeywell, USA, Cat#: AH230)
- ✓ Lyophilized peptide from *Step 3.3.5* in the Procedure section
- ✓ Hydroxypicolinic acid (HPA) (Chem-Impex Int'l Inc., USA, Cat#: 24514)
- ✓ Ammonium citrate (VWR, USA, Cat#: 0470)

Equipment:

- ✓ Wrist action shaker (Burrell, USA, Cat#: 14-400-122)
- ✓ Microcentrifuge (Hettich, Mikro 200, Germany)
- ✓ Centrifuge (Thermo Scientific, Sorvall Legend XTR, USA)
- ✓ Amicon Ultra-0.5 mL centrifugal filters (Millipore Sigma, USA, Cat#: UFC5003BK)
- ✓ Spin-X™ centrifuge tube filters (Millipore Sigma, USA, Cat#: CLS8169)
- ✓ Vortex mixer (VWR, USA, Cat#: 10153-688)
- ✓ UV/Vis Nanodrop detector (Thermo Scientific, Nanodrop One, USA)
- ✓ Matrix-assisted laser desorption ionization time of flight mass spectrometer (MALDI TOF MS) (Bruker, Microflex LRF MALDI, USA)
- ✓ pH meter (Sartorius, pHBasic, Germany)
- ✓ Analytical HPLC (Agilent Technologies, 1220 Infinity LC, USA)

3.2.5 Thiolating Glass Slides

Reagents:

- ✓ Acetone (Millipore Sigma, USA, Cat#: 320110-4L)
- ✓ Sylgard 184 elastomer kit (Fisher Scientific, USA, Cat#: NC9285739)
- ✓ 3-mercaptopropyltrimethoxysilane (MPTS) (Millipore Sigma, USA, Cat#: 175617-100G)
- ✓ Dichloromethane (DCM) (VWR, USA, Cat#: BDH1113-4LG)
- ✓ Ethanol (EtOH) (VWR, USA, Cat#: 89125-188)
- ✓ Deionized (DI) water

Equipment:

- ✓ Glass slides (VWR, USA, Cat#: 48300-026)
- ✓ Glass cutter (Grainger, USA, Cat#: 36M387)
- ✓ Desiccator (Fisher Scientific, USA, Cat#: 08-594-15B)
- ✓ Oven (VWR, USA, Cat#: 89511-408)
- ✓ Kimwipes (Fisher Scientific, USA, Cat#: 06-666A)

3.2.6 Fabricating and Patterning of NorHA Hydrogels

Reagents:

- ✓ NorHA created in *Step 3.3.2* in the Procedure section
- ✓ 2-hydroxy-4'-(2-hydroxyethoxy)-2-methylpropiophenone (I2959) (Millipore Sigma, USA, 410896-50G)
- ✓ Dulbecco's phosphate-buffered saline (PBS) (VWR, USA, Cat#: 45000-434)
- ✓ DL-dithiothreitol (DTT) (Millipore Sigma, USA, Cat#: 43819-1G)
- ✓ Single-stranded DNA (surface and displacement strands, see **Table 3.1**)
- ✓ Peptide-DNA conjugates created in S*tep 3.3.9* in the Procedure section

Equipment:

- ✓ OmniCure® S1500 UV lamp with 320-390 nm filter (Excelitas® Technologies, USA, Cat#: 019-01048R)
- ✓ UV light meter (VWR, USA, Cat#: 97036-010)
- ✓ Vortex mixer (VWR, USA, Cat#: 10153-688)
- ✓ Thiolated glass slides created in S*tep 3.3.10* in the Procedure section

- ✓ Photomask (100 and 200 µm lines and letters “ASU”, CAD/Art Services Inc., USA)
- ✓ Syringe pump (Fisher Scientific, USA, Cat#: 14-831-200)
- ✓ 8-well plates (Fisher Scientific, USA, Cat#: 12-565-497)
- ✓ Fluorescent microscope (DMi8 Leica, USA)

3.2.7 Scaffold Seeding and Culturing

Reagents:

- ✓ Hydrogels created in *Step 3.3.11* and *3.3.12* in the Procedure section
- ✓ Gibco™ minimum essential medium α (MEM) no nucleosides (Fisher Scientific, USA, Cat#: 12-561-072)
- ✓ Gibco™ fetal bovine serum (FBS) (Fisher Scientific, USA, Cat#: 16-000-044)
- ✓ Gibco™ penicillin-streptomycin (pen/strep) (Fisher Scientific, USA, Cat#: 15-140-122)
- ✓ Gibco™ L-glutamine (Fisher Scientific, USA, Cat#: 25-030-081)
- ✓ Dulbecco’s phosphate-buffered saline (PBS), sterile (VWR, USA, Cat#: 45000-434)
- ✓ Gibco™ trypsin-EDTA (Fisher Scientific, USA, Cat#: 25-300-120)
- ✓ Ethanol (EtOH) (VWR, USA, Cat#: 89125-188)
- ✓ Human mesenchymal stromal cells, passage 3 (hMSCs, Lonza, USA, Cat#: PT-2501)

Equipment:

- ✓ Biosafety cabinet (Class II A2, Thermo Scientific, model: 1353, USA)

- ✓ Incubator (VWR, model: VWR51014991, USA)
- ✓ 15 mL sterile conical tubes (Fisher Scientific, USA, Cat#: 12-565-269)
- ✓ 50 mL sterile conical tubes (Fisher Scientific, USA, Cat#: 12-565-271)

Recipes:

- ✓ Cell culture media: αMEM, 16% FBS, 1% pen/strep, 1% L-glutamine

3.2.8 Cell Morphology Staining

Reagents:

- ✓ Dulbecco's phosphate-buffered saline (PBS) (VWR, USA, Cat#: 45000-434)
- ✓ 16% methanol-free paraformaldehyde (PFA) (Fisher Scientific, USA, Cat#: AA433689M)
- ✓ Bovine serum albumin (BSA) (Millipore Sigma, USA, Cat#: A1470-10G)
- ✓ Triton-X 100 (Millipore Sigma, USA, Cat#: T8787)
- ✓ Fluorescein phalloidin (Fisher Scientific, USA, Cat#: F432)
- ✓ 4′,6-diamidino-2-phenylindole (DAPI) (Fisher Scientific, USA, Cat#: D1306)

Equipment:

- ✓ 15 mL sterile conical tubes (Fisher Scientific, USA, Cat#: 12-565-269)
- ✓ 50 mL sterile conical tubes (Fisher Scientific, USA, Cat#: 12-565-271)
- ✓ Vortex mixer (VWR, USA, Cat#: 10153-688)
- ✓ Fluorescent microscope (DMi8 Leica, USA)

3.3 Procedure

3.3.1 HA-TBA Synthesis

1. Let Na-HA warm up to room temperature before use. Dissolve 1-2% Na-HA (5 g bottle) in DI water (250-300 mL) in 500 mL RBF for 1 hour.

   NOTE: Stopper RBF to prevent evaporation.
2. Let ion exchange resin warm up to room temperature. Add 3 g resin / g of Na-HA (15 g per 5 g bottle) to ~100 mL of DI water to make a slurry.
3. Add slurry to HA solution via glass funnel and stir at room temperature for 6 hours.
4. Filter HA solution into a volumetric flask under vacuum using #2 filter paper to remove resin from HA solution.
5. Dilute TBA-OH with DI water at a 1:1 dilution and neutralize HA solution to pH 7.02 to 7.05.

   TIP: Keep 2-3 mL of acidic HA solution in case of overshooting the pH. When adding TBA-OH, start with 1 mL aliquots until pH 5, then reduce to 50 µL and continue reducing TBA-OH volume until reaching the appropriate pH range.
6. Aliquot 45 mL of HA-TBA into 50 mL conical tubes and freeze at -80 °C overnight.
7. Lyophilize for 3-4 days or until completely dry. Store sample at -20 °C.

   TIP: The outside of the sample may look dry but test the center using tweezers to confirm it is completely dry before removing from lyophilizer.
8. Dissolve dry HA-TBA at 2-3 mg/mL in D_2O in an NMR tube. Analyze using ^1H NMR to verify synthesis.

NOTE: The TBA methyl peak area at 0.97 ppm will be used in *Step 3.3.2* to synthesize NorHA.

3.3.2 NorHA Synthesis

CAUTION: All reagent preparation steps described below must be performed in a chemical fume hood. Various hazardous organic solvents, chemicals, and sharps are used in this procedure. Therefore, appropriate personal protective equipment (i.e. lab coat, gloves, and protective glasses) should be used. It is highly advised to read the SDS for each chemical.

1. Remove 250 mL RBF with stir bar from the oven, stopper immediately and let cool.

   NOTE: The RBF and stir bar must be completely dry before use since water terminates the reaction. It is recommended to store in the oven overnight.
2. Let HA-TBA and BOP warm up to room temperature. Using HA-TBA weight and NMR results from *Step 3.3.1-8*, calculate the amount of nor-amine and BOP needed to reach desired norbornene functionalization.

   TIP: Desired norbornene functionalization should be greater than 60%. This becomes important in S*tep 3.3.11* and *3.3.12*, especially when tethering more than one DNA strand to the hydrogel.
3. Add HA-TBA and nor-amine to RBF and stopper immediately.
4. Add anhydrous DMSO (~5 mL per 0.1 g HA-TBA) to RBF via cannulation using nitrogen gas. Stir at 350-400 rpm and fully dissolve HA-TBA before continuing.

NOTE: During cannulation, vent the system with 22 ga needles. Once cannula and needles are removed, cover the holes with electrical tape.

CAUTION: Pressure can build up throughout the system if the nitrogen gas flow rate is too high. Insert a bubbler into the system to visually check on flow rate.

5. Remove 100 mL RBF with stir bar from oven, stopper immediately and let cool.

   NOTE: The RBF and stir bar must be completely dry before use since water terminates the reaction. It is recommended to store in the oven overnight.

6. Add BOP and stopper immediately.
7. Add ~20 mL anhydrous DMSO to BOP via cannulation, dissolve BOP completely, and cannulate into the HA solution.

   NOTE: The solution will turn from light pink to a translucent yellow.

   NOTE: During cannulation, vent the system with 22 ga needles. Once cannula and needles are removed, cover the holes with electrical tape.

   TIP: Rinse cannula with acetone and return to oven directly after use to prevent clogging.

8. Allow HA solution to react for ~2 hours stirring at 350-400 rpm at room temperature to form NorHA.
9. Soak dialysis tubing in DI water for 30 minutes and rinse thoroughly to remove any glycol residue.
10. After the reaction time, quench NorHA solution with ~10 mL cold DI water, transfer to the pre-soaked dialysis tubing, and seal dialysis tubing with clips.
11. Purify NorHA solution via dialysis using 3 L of DI water for 5 days at room temperature.

TIP: Add ~5 g NaCl to DI water for the first 3 days. Change DI water twice daily.

12. Filter NorHA solution using a 40 µm cell strainer to remove side products from BOP coupling. Return to dialysis for another 3-5 days.
13. Remove NorHA solution from dialysis and adjust to pH 7 using 0.1 or 1 M NaOH. Aliquot NorHA solution to 50 mL conical tubes and freeze at -80 °C overnight.

    CRITICAL STEP: The NorHA solution must be at a pH of 6.9-7.1 to prevent crosslinking with itself.
14. Lyophilize for 3 days or until completely dry. Store sample at -20 °C.

    TIP: The outside of the sample may look dry but test the center using tweezers to confirm it is completely dry before removing from lyophilizer.
15. Dissolve dry NorHA at 2-3 mg/mL in D_2O in an NMR tube. Analyze using ^1H NMR to determine norbornene functionalization.

    NOTE: Functionalization of the four norbornene peaks from 6.02 to 6.33 ppm will be used in S*tep 3.3.11* to fabricate NorHA hydrogels. If TBA peaks are still present, additional dialysis is needed.

3.3.3 Peptide Synthesis

CAUTION: All reagent preparation steps described below must be performed in a chemical fume hood. Various hazardous organic solvents and chemicals are used in this procedure. Appropriate personal protective equipment (i.e. lab coat, gloves, and protective glasses) should be used, and it is highly advised to read the SDS for each chemical.

NOTE: Each amino acid can be single-coupled or double-coupled, depending on the nature of the amino acid. For sterically hindered amino acids (e.g., Fmoc-Ile-OH, Fmoc-Asn(Trt)-OH, Fmoc-Cys(Trt)-OH, Fmoc-Gln(Trt)-OH, Fmoc-Arg(Pbf)-OH, Fmoc-Val-OH, Fmoc-Thr(tBu)-OH, and amino acids coupled subsequently to a Pro residue, double coupling is needed. Double coupling the amino acids is especially necessary if the peptide chain is longer than 20 amino acids. For the synthesis of the RGDS peptide, every amino acid was double coupled to ensure a high coupling efficiency.

1. Prepare each amino acid at a concentration of 0.2 M in DMF. Cap and vortex the solution for one minute.

   NOTE: The amount of each amino acid solution is going to vary, depending on the frequency of the amino acid present in the desired peptide.

   TIP: Fmoc-amino acids are stable in DMF for two weeks.
2. Prepare a 25 mL deprotection solution by adding 7 mL of piperidine in 18 mL of DMF in a 250 mL glass bottle with a screw-on cap.

   CAUTION: Piperidine is highly flammable and toxic.

   TIP: Deprotection solution is stable in DMF for one month.
3. Prepare 17 mL of an activator solution by pipetting 1.32 mL DIC in 15.68 mL of DMF in a 250 mL glass bottle with a screw-on cap.

   TIP: Activator solution is stable in DMF for one week.

4. Prepare 9 mL of an activator base solution by weighing out 1.28 g of Oxyma, pipetting 0.16 mL of DIEA, and diluting the solution with 7.56 mL of DMF in a 250 mL glass bottle with a screw-on cap.

   TIP: Activator base solution is stable in DMF for one week.

5. Weigh out the rink amide AM resin and put in the peptide synthesis reaction vessel.

   NOTE: The amount of resin used for the synthesis scale will depend on the loading capacity of the resin.

6. Place all the amino acid solutions into their corresponding spots on the peptide synthesizer and tighten firmly. Place all other solutions (deprotection, activator, activator base) into their corresponding spots.

   TIP: Ensure that the DMF main wash bottle is full, and the waste bottle is empty.

7. Execute peptide synthesis.
8. Once the synthesis is complete, decant the resin into a fritted, cleavage vessel and wash twice with 5 mL of DMF.
9. Wash the resin 3x with 5 mL of DCM for each wash. Allow the resin to dry at room temperature for 10 minutes.

3.3.4 Peptide Cleavage

1. Create a TFA cleavage solution (5 mL per 100 mg of resin), consisting of 9 mL of TFA, 0.25 mL of TIS, 0.50 mL of DODT (half this amount if the peptide does not contain a cysteine), and 0.25 mL of ultrapure water.

   CAUTION: TFA is highly corrosive.

2. Add the TFA cleavage solution to the dried peptide resin and gently agitate the solution for 4 hours at room temperature. Filter the cleavage solution into a 50 mL centrifugal tube.
3. Wash the resin with 2 mL of TFA, agitate for 1 min, and filter the cleavage solution into the same 50 mL centrifugation tube.
4. Allow Et_2O to cool at -20 °C for at least 10 minutes.

   TIP: The volume of Et_2O should be at least 10 times the volume of the concentrated cleavage solution.
5. Precipitate the peptide by adding the precooled Et_2O to the cleavage solution. Allow the precipitated solution to sit at -80 °C for 30 minutes to enhance the precipitation.

   TIP: For better precipitation of the synthesized peptide, evaporate most of the TFA by blowing nitrogen gas over the filtrate in a chemical fume hood before adding Et_2O.
6. Centrifuge precipitated peptide at 7,000×g for 10 minutes at 4 °C.
7. Decant the supernatant into a waste container and allow the crude peptide pellet to air dry in the open conical tube overnight in a chemical fume hood.

3.3.5 Peptide Purification

1. Resuspend the peptide pellet in a 15 mL mixture of water/ACN with 0.1% TFA.

   TIP: The amount of ACN with 0.1% TFA added into the mixture will depend on the hydrophobicity of the peptide. More hydrophobic peptides will require a higher ratio of ACN with 0.1% TFA.

2. Filter the peptide solution using a PVDF membrane filter (25 mm x 0.2 µM).

   CRITICAL STEP: The peptide solution must be filtered through a hydrophobic membrane filter before the sample is injected into the HPLC for purification. Any unfiltered, insoluble impurities may clog the HPLC lines upon injection.
3. Purify the crude peptide using a semipreparative HPLC.
4. With each fraction corresponding to the main peak, confirm the presence of the target peptide using MALDI-TOF MS.
5. Consolidate each pure peptide fraction and freeze at -80 °C.
6. Lyophilize the frozen peptide solution overnight to obtain the purified peptide.

3.3.6 DNA-DBCO Modification

1. Order a 1 µmole scale of amine-modified oligonucleotide from Integrated DNA Technologies, Inc.

   NOTE: Which end of the oligonucleotide (5' or 3') bears the amine modification depends on the use and directionality of the conjugate.
2. Solubilize the DNA to create a 1X PBS, pH 7.5 solution at a total volume of 1 mL. Vortex and incubate the DNA solution at 42 °C in a water bath for 20 minutes.
3. Dissolve 5 mg NHS-Sulfo-DBCO in 94 µL of DMSO to create four 20 µL aliquots of 100 mM NHS-Sulfo-DBCO.
4. Add two 20 µL aliquots of the NHS-Sulfo-DBCO to the DNA solution and let the mixture react with agitation at room temperature for 4 hours.

5. Add two more 20 µL aliquots to the DNA solution and continue the reaction under agitation at room temperature overnight.
6. Filter precipitated/hydrolyzed DBCO with a SpinX centrifugal tube and collect the filtrate using a benchtop centrifuge at 4445×g for 5 minutes.

   CRITICAL STEP: The DNA solution must be filtered through a hydrophobic membrane filter before the sample is injected into the HPLC for purification. Any unfiltered, insoluble impurities may clog the HPLC lines upon injection.
7. Remove unreacted/hydrolyzed NHS-Sulfo-DBCO and other salts with a 0.5 mL 3 kDa MWCO filter.

   TIP: Make sure the DNA has a molecular weight over 4000 Da. Otherwise, use a desalting column.
8. Rinse the DNA-DBCO 6 times with Nanopure water using a benchtop centrifuge at 4445×g for 5 minutes.
9. Transfer the DNA-DBCO solution to a new tube and dilute it with 100 µL of Nanopure water for purification preparation.

   TIP: The DNA-DBCO crude solution should have a slightly yellow tint due to the modification of the DBCO moiety.

3.3.7 DNA-DBCO Purification

1. Purify the DNA-DBCO solution using an analytical HPLC.
2. With each fraction corresponding to the main DBCO peak, consolidate them and concentrate the DNA-DBCO sample in a 4 mL 3 kDa MWCO filter.

TIP: The first peak is the unmodified DNA. The second peak is the DBCO-DNA conjugate, which has an additional UV-Vis absorbance band at 309 nm compared with the unmodified DNA.

3. Once the volume is ~500 µL, concentrate the sample further using a 0.5 mL 3 kDa MWCO filter.
4. Determine the concentration of the DNA-DBCO oligonucleotide based on the extinction coefficient at 260 nm.

   TIP: The DNA-DBCO oligonucleotide should have a slightly yellow tint, due to the modification of the DBCO moiety.

3.3.8 Peptide-DNA Conjugation

1. Dissolve 2-3 mg of the RGDS peptide in 500 µL of Nanopure water.
2. Determine the concentration of the peptide solution based on the extinction coefficient at 280 nm.

   TIP: Here is a link to an online calculator that provides the extinction coefficient as a function of peptide sequence: https://web.expasy.org/protparam/.
3. Dilute the peptide sample to create a 500 µL sample at 1 mM.
4. For the conjugation reaction, mix the DNA-DBCO stock sample and the peptide sample (at a three-fold molar excess) with 100 µL of 10X PBS (pH 7.5). Then dilute the sample to 1 mL with Nanopure water.

   CRITICAL STEP: The peptide is set to be at a 3-fold molar excess. The amount of peptide added will depend on the purification yield of the DNA-DBCO strand. For heavily cationic peptides, lower the DNA-DBCO:peptide molar ratio to 1:2 to

avoid precipitation due to nonspecific aggregation, which lowers the yield of the conjugation reaction.

TIP: If solubility is an issue, add ACN or dilute the sample further with 1X PBS.

5. Incubate the conjugation reaction at 37 °C overnight.
6. Filter off any precipitated peptide-DNA conjugate with a SpinX centrifugal tube and collect the filtrate using a benchtop centrifuge at 4445×g for 5 minutes.

   CRITICAL STEP: The peptide-DNA solution must be filtered through a hydrophobic membrane filter before the sample is injected into the HPLC for purification. Any unfiltered, insoluble impurities may clog the HPLC lines upon injection.
7. Remove any excess peptide and other salts with a 0.5 mL 3 kDa MWCO filter.

   NOTE: Make sure the DNA has a molecular weight over 4000 Da. Otherwise, use a desalting column.
8. Rinse the peptide-DNA conjugate 6 times with Nanopure water using a benchtop centrifuge at 4445×g for 5 minutes.
9. Transfer the peptide-DNA solution to a new tube and dilute it with 100 µL of Nanopure water for purification preparation.

3.3.9 Peptide-DNA Purification

1. Purify the peptide-DNA conjugate using an analytical HPLC.
2. Consolidate each fraction corresponding to the main peptide-DNA peak and concentrate the solution in a 4 mL 3 kDa MWCO filter at 4445×g.

TIP: The first peak will be the DNA-DBCO. The major peak corresponds to the conjugate. If conjugation was not efficient, there will be another peak associated with DNA-DBCO which will have a larger absorbance at 309 nm.

3. Once the volume is ~500 µL, concentrate the sample further using a 0.5 mL 3 kDa MCWO filter.
4. Determine the concentration of the peptide-DNA conjugate based on the extinction coefficient of the DNA at 260 nm.

3.3.10 Thiolated Glass Slides

1. Use glass cutters to make 1x1 inch glass slides. Wipe with acetone.
2. Mix Sylgard 184 components at 10:1 (base:catalyst) with 10 µL of MPTS per 1 g of base.
3. Place in a desiccator under vacuum for 1-2 minutes to remove bubbles.

   CRITICAL STEP: Do not leave under vacuum for too long otherwise the MPTS will keep the solution from fully curing.
4. Add a thin coat of the mixture to the glass slides.
5. Bake at 125 °C for 1 hour.

   CAUTION: Oven needs to be ventilated to remove MPTS vapors.
6. Remove glass slides and place in chemical fume hood. Wash with DCM, EtOH, and DI water sequentially.
7. Dry with a Kimwipe and store under vacuum.

3.3.11 Fabricating NorHA Hydrogels

1. Let lyophilized NorHA warm up to room temperature before use. Calculate the amount of NorHA, I2959 (0.05% in PBS), and DTT (0.5 M) needed to make hydrogels at the desired polymer concentration and crosslinking density using the functionalization percentage determined in *Step 3.3.2-15*. For example, 10 mg NorHA (60% functionalization), 247.34 µL 0.05% I2959, and 2.66 µL 0.5 M DTT is needed to make a 4% NorHA solution with 20% of norbornene groups consumed for crosslinking.

   CRITICAL STEP: Do not crosslink hydrogels using more than 50% of the available norbornene groups. Sufficient norbornene groups must be remaining for S*tep 3.3.12*.

   NOTE: If using hydrogels for cell work, add a low concentration of a cell adhesion peptide in bulk to promote cell attachment (i.e. 10 µM RGDS).
2. Vortex NorHA, I2959, and DTT until fully dissolved.
3. Pipette NorHA solution into each silicone mold (diameter: 4.5 mm, height: 2 mm) and cover solution with a thiolated glass slide from S*tep 3.3.10*.
4. Expose to UV light for 5 minutes at 10 mW/cm^2. Carefully remove from the mold.

   CAUTION: UV light can cause eye damage. Wear safety glasses that protect against UV light.

3.3.12 Patterning NorHA Hydrogels

NOTE: Nomenclature for different single-stranded DNA (ssDNA) is as followed: surface (S), complementary biomolecule (cB), and complementary displacement (cD).

1. Prepare a S DNA solution in I2959 (0.05% in PBS) at desired concentration. For example, 50 μM S DNA was used to demonstrate spatial control and 100 μM S DNA was used with peptide-DNA conjugates to demonstrate bioactivity.

   NOTE: This DNA strand will be irreversibly tethered to the hydrogel surface.
2. Add 5 μL S DNA solution to each hydrogel surface and allow diffusion into the hydrogel for 5 minutes.
3. Remove excess liquid and place photomask on top of the hydrogel.
4. Expose hydrogel to UV light for 60 seconds at 10 mW/cm^2. Carefully remove mask.

   NOTE: If patterning a gradient, use a sliding photomask that is actuated by a syringe pump (**Figure 3.1**) at desired speed for desired time.

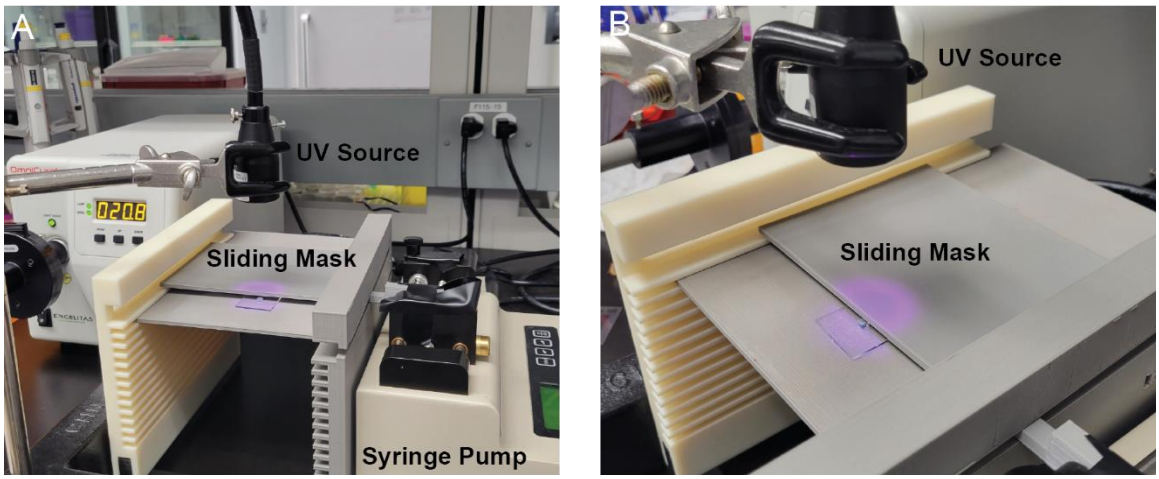

Figure 3.1: Setup for sliding photomask from (A) front and (B) top view.

5. Place hydrogels in an 8-well plate and rinse 3x for 5 minutes in PBS, then incubate in PBS overnight.
6. Aspirate PBS. Prepare a cB DNA solution in PBS at the same concentration as the S DNA solution.
7. Add cB DNA solution to each hydrogel and incubate for 5-10 minutes. If a fluorophore is present, protect from light to prevent photobleaching.
8. Wash samples with PBS for at least 1 hour with multiple PBS exchanges to remove excess cB DNA.
9. If desired, image samples using a fluorescent microscope.

   TIP: Make note of the camera settings (ex: exposure time, gain, etc.) to use for future imaging of the same samples.
10. To remove cB DNA from the surface, prepare a cD DNA solution at 2x the concentration of the cB DNA concentration.

11. Add to the hydrogel surface and incubate for 30-60 minutes. If a fluorophore is present, protect from light to prevent photobleaching.
12. Wash samples with PBS for at least 1 hour with multiple PBS exchanges to remove cB-cD DNA complex.
13. If desired, image samples using a fluorescent microscope with the same settings in step 9.
14. Repeat steps 6-13 to turn biomolecule signal "ON" and "OFF" as desired.

3.3.13 Scaffold Seeding and Cell Culture

NOTE: All steps must be done in a biosafety cabinet and protected from light as much as possible.

1. Sterilize hydrogels made in *Step 3.3.12* by soaking in 70% EtOH for 30 minutes.
2. Rinse hydrogels 3-5x for 10 minutes each with sterile PBS.
3. Detach cells from flask using trypsin and resuspend in media.
4. Seed cells onto hydrogel surfaces at 5,000 cells/cm^2 (or other desired concentration).
5. Culture cell-seeded hydrogels in an incubator at 37 °C and 5% CO_2. Change media every 2-3 days.

   TIP: Add and remove media slowly to avoid disturbing the cells or the hydrogel.
6. To add the peptide-DNA conjugate at a desired time point, aspirate media and prepare a peptide-DNA solution in sterile PBS at the desired concentration. Add 5 µL to each hydrogel surface and incubate for 5-10 minutes at 37 °C. Rinse with warm, sterile PBS before adding media and place in the incubator.

7. To remove the peptide-DNA conjugate at a desired time point, aspirate media and prepare a cD DNA solution in sterile PBS at the desired concentration. Add 5 µL to each hydrogel surface and incubate for 30 minutes at 37 °C. Rinse with warm, sterile PBS before adding media and place in the incubator.

3.3.14 Cell Morphology Staining

NOTE: If a fluorophore is present, protect hydrogels from light during all steps to prevent photobleaching.

1. Remove cell-seeded hydrogels from incubator, aspirate media, and wash hydrogels with PBS.
2. Fix hydrogels in 4% PFA for 30-45 minutes. Rinse 2-3x with PBS.
3. Prepare a 0.1% Triton-X 100 solution in PBS, add to the hydrogel, and incubate at room temperature for 15 minutes. Rinse 2-3x with PBS.
4. Prepare a 5% BSA solution in PBS, add to the hydrogel, and incubate at room temperature for 45 minutes.
5. Aspirate BSA solution, add fluorescein phalloidin (1 µM in BSA solution), and incubate at room temperature for 1 hour.
6. Aspirate fluorescein phalloidin, add DAPI (300 nM in BSA solution), and incubate at room temperature for 10 minutes. Rinse hydrogels 3x in PBS for 5 minutes each.
7. Image cells using a fluorescent microscope.

3.4 Results

3.4.1 HA-TBA and NorHA Synthesis

HA-TBA and NorHA synthesis was confirmed using ^{1}H NMR. Proton peak assignments for HA-TBA and NorHA are based on published spectra.[19,76,77] The NMR spectra for both HA-TBA and NorHA were normalized to the methyl peak at 2.06 ppm (3H, CH3, a). NMR showed successful addition of TBA to HA with proton peaks corresponding to TBA at chemical shifts between 0.5 and 3.5 ppm (**Figure 3.2**). These chemical shifts include: 0.98 ppm (CH3, b), 1.4 ppm (CH2, c), 1.69 ppm (CH2, d), and 3.23 ppm (CH2, e). The TBA methyl peak area at 0.98 ppm was used to calculate the ratio of HA to TBA and the corresponding molecular weight of the HA-TBA repeat units to determine the amount of nor-amine and BOP needed to synthesize NorHA.

The disappearance of the TBA peaks (**Figure 3.2**, b-e) and the addition of the norbornene peaks (**Figure 3.3**) between 6.0 and 6.3 ppm (2H, C=C, b), 2.87 ppm (CH2, c), and 1.3 to 1.43 ppm (CH2, d) confirmed successful conjugation of norbornene to the carboxyl groups on HA via an amidation reaction. If the NMR shows excess TBA after dialysis, continue dialysis until TBA is no longer present in the NMR spectra. The area of the four vinyl proton peaks between 6.0 and 6.3 ppm was used to determine the percent functionalization of norbornene within HA. **Figure 3.3** shows ~68% of the disaccharide repeat units within HA were modified with norbornenes.

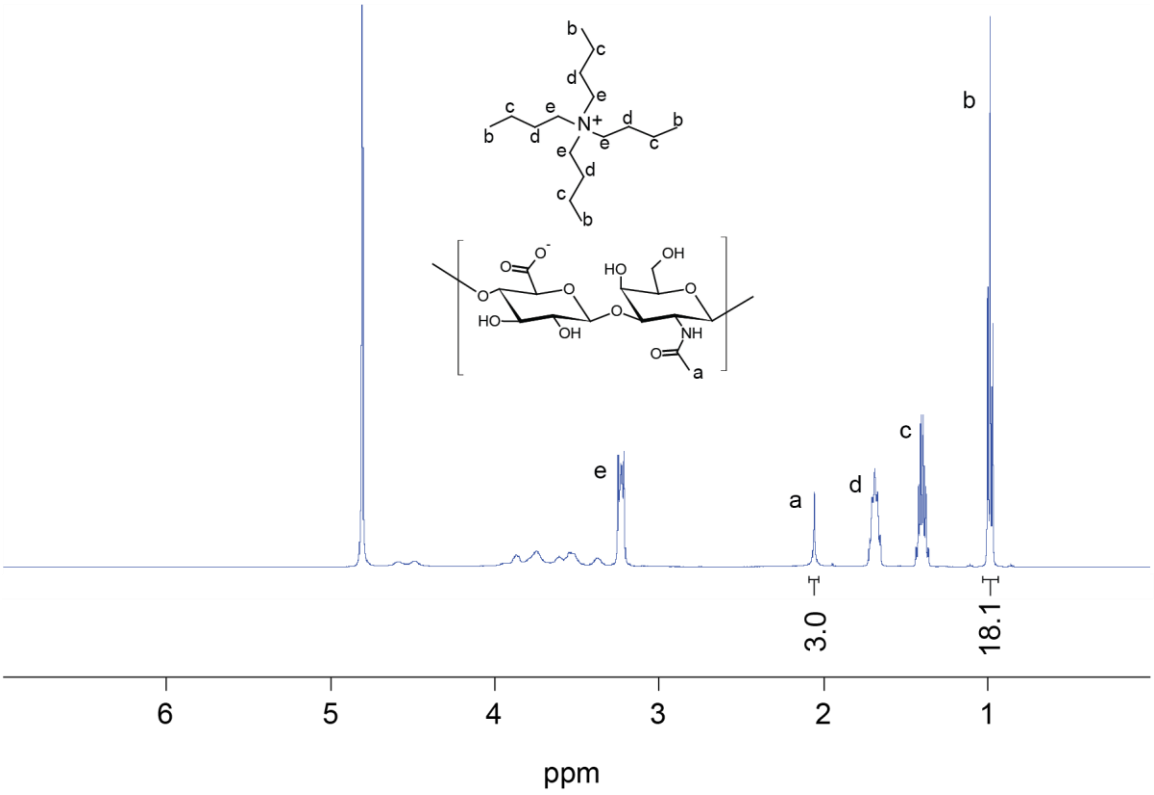

Figure 3.2: ^{1}H NMR (500 MHz, D_2O) and corresponding chemical structure of HA-TBA.

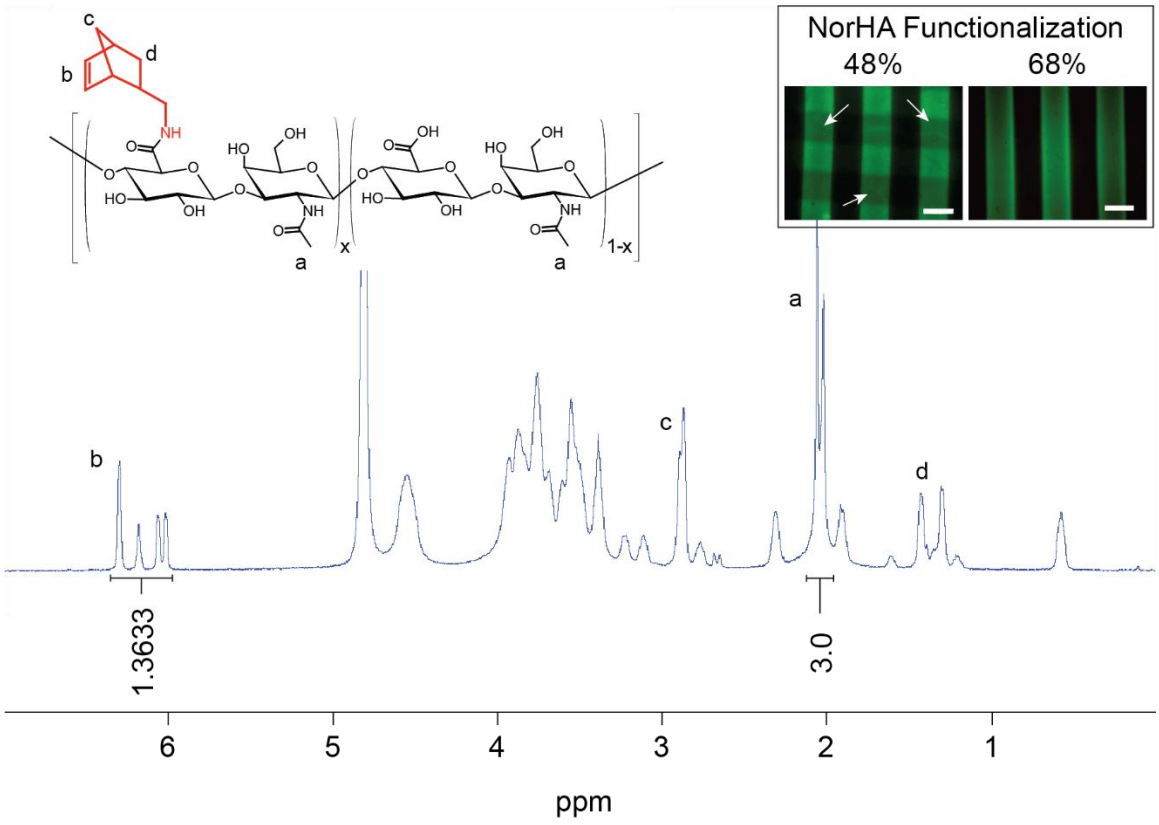

Figure 3.3: ^{1}H NMR (500 MHz, D_2O) and corresponding chemical structure of NorHA. ^{1}H NMR spectrum shows that ~68% of the carboxylic acid groups were modified with norbornene groups. High norbornene functionalization is necessary when tethering multiple biomolecules to ensure uniform patterning (inset). Scale bar = 200 μm.

3.4.2 Spatiotemporal Control of DNA Conjugates on NorHA Scaffolds

Six distinct ssDNA sequences were used to assess the specificity of DNA and how it can be used as a reversible linker: surface DNA strand (S), complementary biomolecule-DNA strand with toehold region (cB), and complementary displacement DNA strand with toehold region (cD) with (1) fluorescein and (2) rhodamine on the cB strands. The DNA sequences for each strand are listed in **Table 3.1**. These DNA linkages were tested to confirm their ability to spatiotemporally control biomolecule presentation via toehold-mediated strand displacement (**Figure 3.4**). The S DNA strands are placed on

top of the hydrogel surface and undergo radical-mediated photoconjugation when exposed to UV light, tethering them to the hydrogel. Then cB strands are introduced to form a duplex with the S strands, with the toehold region remaining single-stranded. Lastly, cD strands are introduced, which bind to the toehold region of the cB strand and outcompete the S strands via branch migration to fully remove the cB strands.

Various photomasks were used to demonstrate the spatial control of DNA patterning afforded by this platform. **Figure 3.5A-C** displays patterned line widths of 100 and 200 μm as well as the letters "ASU." Fluorescence intensity as a function of the hydrogel width (yellow dashed line) was representative of the spatial resolution possible via photopatterning (**Figure 3.5A, B inset**). To spatiotemporally control biomolecule presentation, S1 was spatially tethered to the surface using a photomask with 200 μm thick lines. Then, cB1 was added to turn the signal "ON" (**Figure 3.5D**); removal of cB1 using cD1 then turns the signal "OFF" (**Figure 3.5E**). Following rinsing and removal of the cB1-cD1 duplex, a fresh batch of cB1 was added to the free S strand to turn the signal "ON" again (**Figure 3.5F**), verifying spatiotemporal control of a single signal.

To demonstrate independent spatiotemporal control of two signals, the same steps were repeated using a photomask with 200 μm thick lines to create a crosshatch pattern. Briefly, 1) S1 was tethered to the hydrogel and washed extensively, 2) S2 was tethered to the hydrogel and washed extensively, and 3) cB1 and cB2 were added to the hydrogel. This layout resulted in four distinct areas (**Figure 3.6A**): cB1 only (red), cB2 only (green), both cB1 and cB2 (yellow), and no signals (black). Once again, each signal was added and removed using its respective cB and cD strands, demonstrating precise and independent spatiotemporal control over each biomolecule (**Figure 3.6B, C**). More

complex spatial patterning was possible by using a sliding photomask to create gradients. S1 and S2 were patterned sequentially at 90° angles to one other, and cB1 and cB2 strands were added to create quadrants of high/low (Q1), low/low (Q2), low/high (Q3), and high/high (Q4) concentrations, respectively (**Figure 3.6D**). The corresponding cB and cD strands were used to add or remove each signal specifically resulting in only one signal present (**Figure 3.6E, F**). Fluorescence intensity profiles (yellow dashed line = cB1, white dashed line = cB2) show the change in fluorescence along the gradient with the signal being reduced at the halfway point of the hydrogel (**Figure 3.6G-I**).

Together, these results demonstrate how easily a wide variety of patterns can be created using a UV light-mediated method while incorporating DNA as a linker to provide full reversibility and orthogonal control of two signals. The addition of using a sliding photomask to create more complex patterns is more representative of the natural biochemical gradients found throughout the human body.[78–80] An additional benefit of using gradient patterns in an *in vitro* model is the ability to perform high throughput screening for optimal biomolecule concentrations on the surface of a single hydrogel. For example, Vega et al. used NorHA to create spatially controlled biochemical gradients to study the relationship between a wide range of biomolecule concentrations and chondrogenesis.[19]

Table 3.1: DNA sequences for surface (S), complementary biomolecule (cB), and complementary displacement (cD) DNA strands for fluorescein (1) and rhodamine (2).

Name	DNA Sequence (5'→3')
Fluorescein	
S1	HS-AGTTTCGTCCAACGCTCAAGAAC
cB1	Fluorescein-TTTTTGTTCTTGAGCGTTG
cD1	CAACGCTCCAGAACAAAAA
Rhodamine	
S2	HS-TCATCTACGTTGAACCTGCCACA
cB2	Rhodamine-AAAAATGTGGCAGGTTCAA
cD2	TTGAACCTGCCACATTTTT

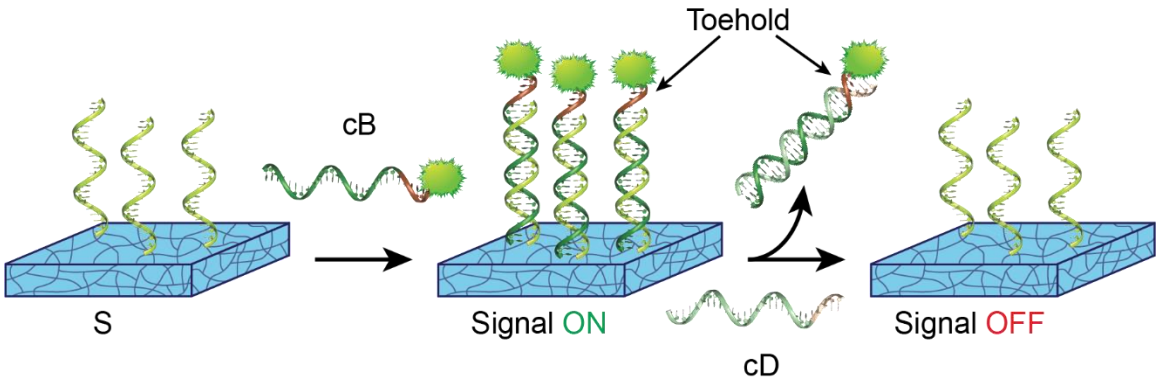

Figure 3.4: Schematic of toehold-mediated strand displacement. Strand S is tethered to the hydrogel surface (left). cB DNA with a toehold region (brown) is introduced and forms a duplex with the S strand turning the signal "ON" (middle). cD DNA that is fully complementary to cB binds to the toehold region and outcompetes the S strand to remove the cB strand, turning the signal "OFF" (right).

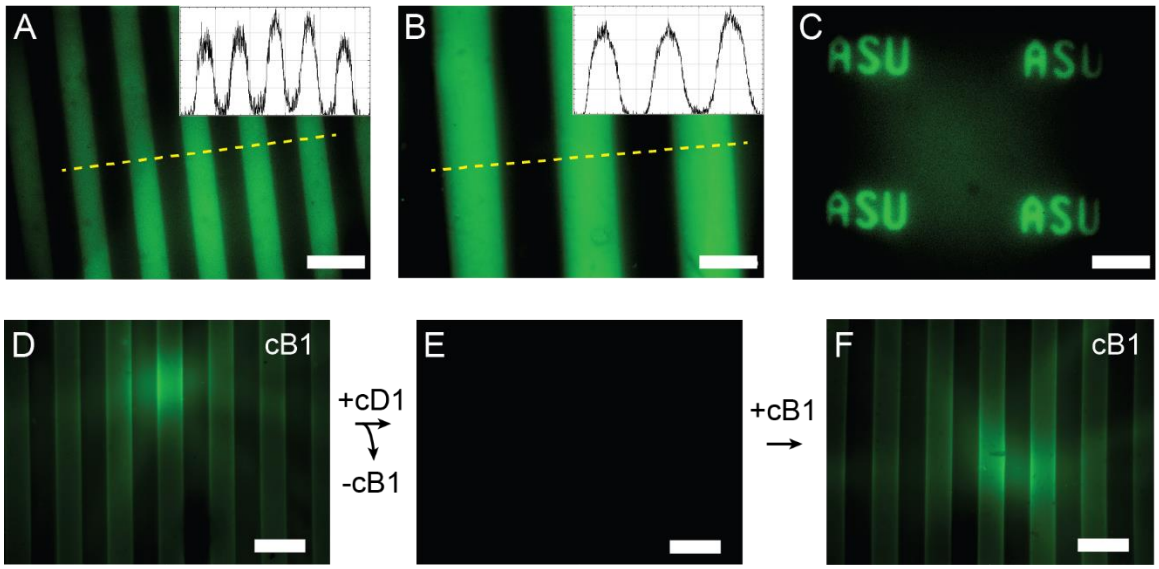

Figure 3.5: Patterning DNA handles on photoresponsive NorHA creates a fully reversible, spatiotemporally defined hydrogel platform. (A-C) NorHA enables spatial control of the biomolecule signal via photomasks to create the following shapes: (A) 100 and (B) 200 μm lines and (C) the letters "ASU" with pattern fluorescence intensity profiles acquired over the dashed yellow line (A, B inset). (D-F) To demonstrate spatiotemporal control, strands S1, cB1, and cD1 were used to have cB1 present or absent from the surface. Scale bar = (A-C) 200 μm, (D-F) 400 μm.

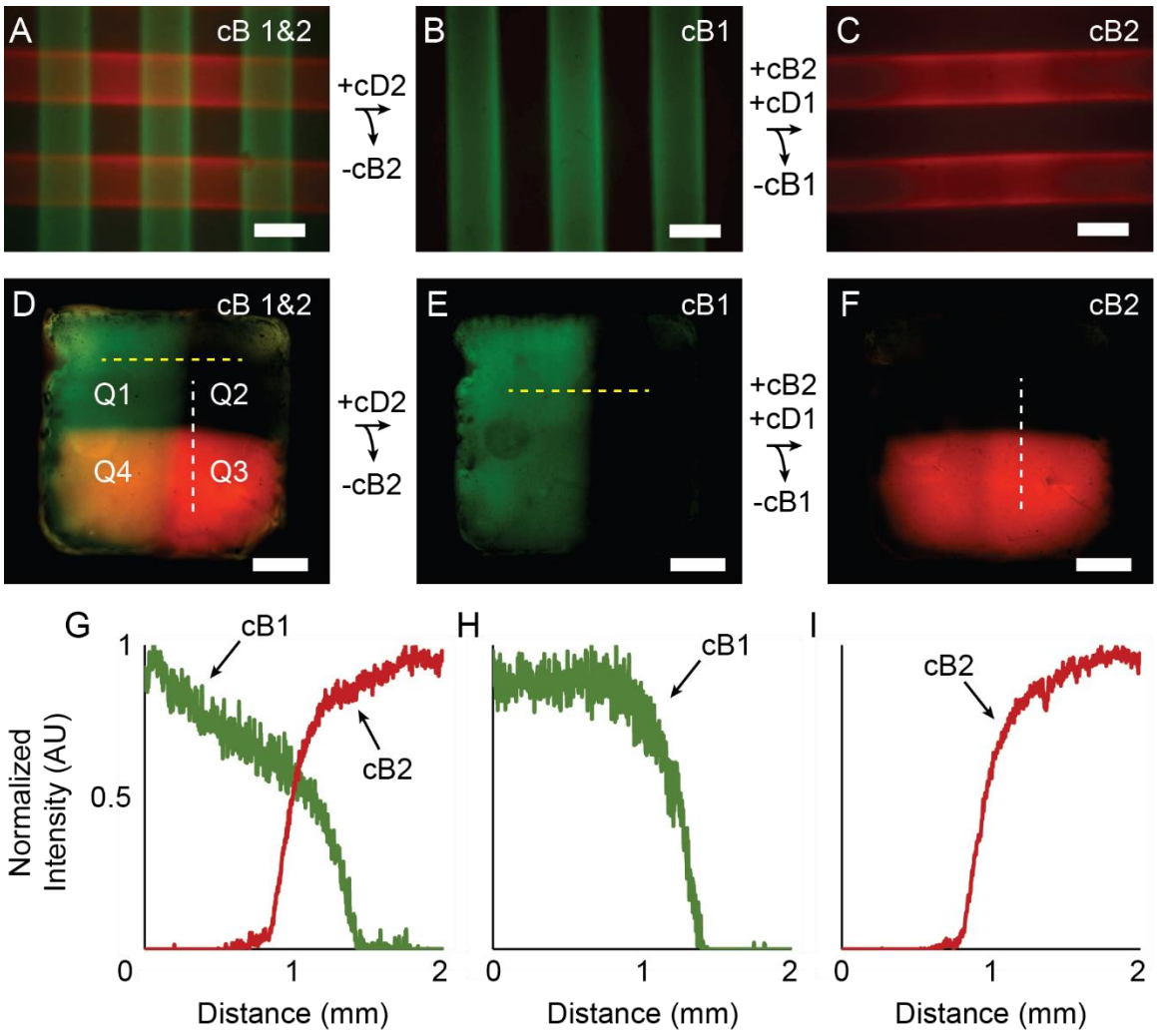

Figure 3.6: DNA-NorHA hydrogels support orthogonal spatiotemporal control of multiple biomolecule signals. To demonstrate independent spatial and temporal control of two signals, (A) S1-cB1 and S2-cB2 were photopatterned perpendicular to each other to form a crosshatch pattern. (B) cB1 remained when cB2 was removed via cD2 addition. (C) cB1 was removed and cB2 was readded by simultaneously introducing cD1 and cB2, respectively. (D-I) The process was repeated using a sliding photomask to create (D-F) complex gradients with (G-I) fluorescence intensity profiles for cB1 (yellow dashed line) and cB2 (white dashed line). Scale bar = (A-C) 200 μm, (D-F) 1 mm.

3.4.3 Synthesis of RGDS and RGDS-DNA Conjugates

The cell-matrix mimetic peptide RGDS (full sequence: ZGYG**RGDS**PG) and RGDS conjugated to the cB2 DNA strand were synthesized using the peptide synthesis

and peptide-DNA conjugation protocols described previously. Once synthesized and cleaved, the peptide was readily purified by reverse-phase HPLC and characterized by MALDI-TOF MS (*m/z*). The expected mass for the RGDS peptide was *m/z* 1017 Da and was confirmed with MALDI-TOF MS where there was a clear mass peak at *m/z* 1020 Da (**Figure 3.7A).** Then the peptide was conjugated to the cB2 DNA (**Table 3.1**) sequence and purified using reverse-phase HPLC. The peptide-DNA conjugate was confirmed with MALDI-TOF MS with the expected mass being *m/z* 8406 Da and the actual mass peak at *m/z* 8445 Da (**Figure 3.7B**).

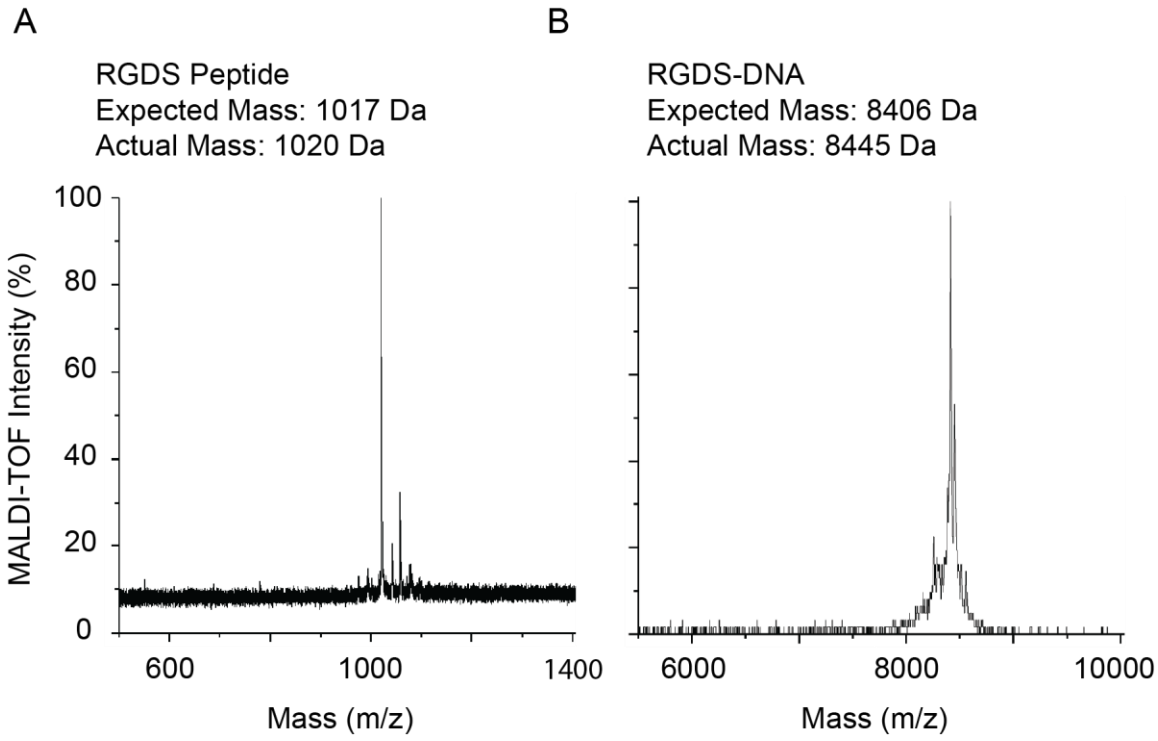

Figure 3.7: MALDI mass spectra for RGDS peptide and RGDS-DNA conjugate.

3.4.4 Cell Morphology Changes with RGDS-DNA Presentation

Human mesenchymal stromal cells (hMSCs) were cultured for 3 and 7 days to demonstrate RGDS-DNA can be removed at longer culture times, and the DNA was not degraded or occluded by secreted proteins. NorHA hydrogels were synthesized with 10 μM of RGDS within the bulk hydrogel to prevent hMSCs from detaching from the surface once RGDS-DNA was displaced. Then, 100 μM of RGDS-DNA was added to the hydrogel surface via DNA hybridization with the complementary DNA strand tethered to the hydrogel surface. The hydrogels were sterilized with ethanol, cells were seeded onto the surface, and the cell-seeded hydrogels were incubated at 37 °C. Once seeded, hMSCs were cultured for either 3 or 7 days. On day 3, a third of the samples were fixed and stained to determine cell morphology after three days of RGDS signaling (**Figure 3.8A**). Half of the remaining samples were treated with cD strands to displace the RGDS-DNA while RGDS-DNA remained bound to the other half of the samples, and both were cultured for another 4 days. On day 7, all remaining samples were fixed and stained. Cells on hydrogels where RGDS remained bound to the surface remained spread (**Figure 3.8B**) while cells on hydrogels where RGDS was removed contracted (**Figure 3.8C**). The effects are further noticed when comparing the cell area (**Figure 3.8D**) and aspect ratio (**Figure 3.8E**). There was a slight increase in cell area when hMSCs were cultured until day 7 with RGDS present compared to day 3, while the aspect ratio roughly remained the same. However, there was a statistically significant decrease in cell area and aspect ratio when RGDS-DNA was removed at day 3.

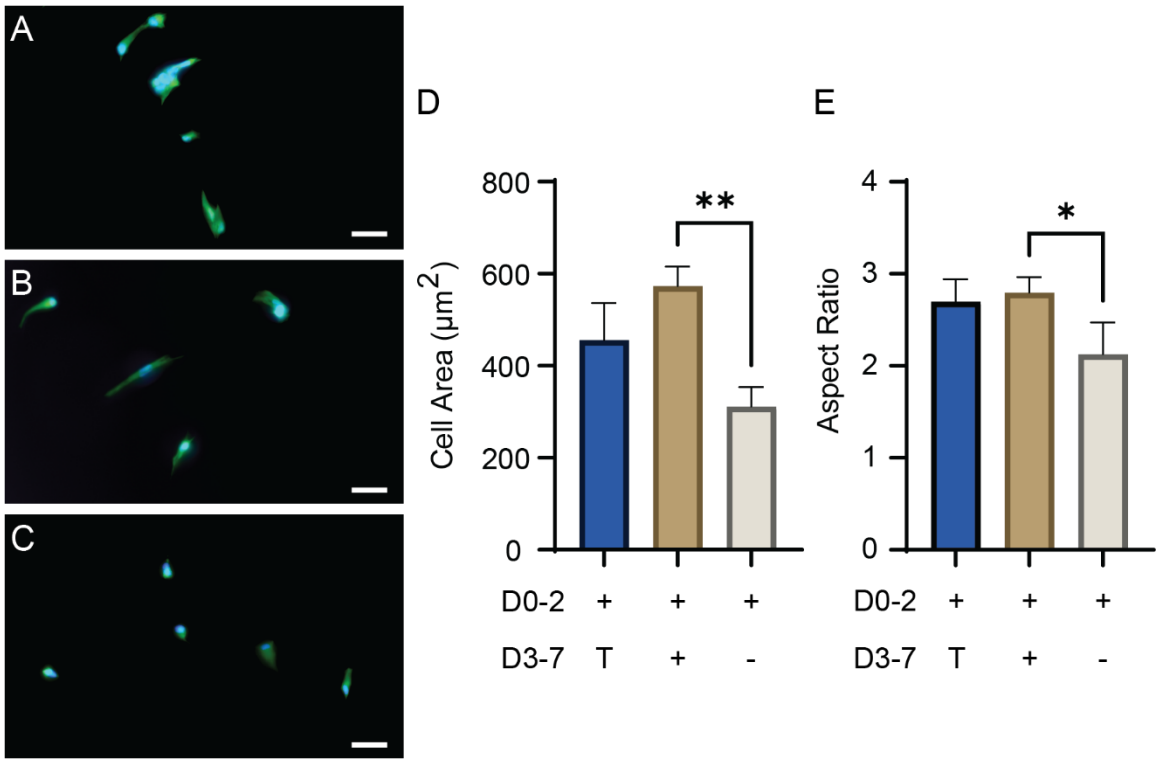

Figure 3.8: Cell morphology changes with the addition and removal of RGDS-DNA. (A-B) In the presence of RGDS-DNA, hMSCs were spread at (A) day 3 and (B) day 7. (C) However, hMSCs contracted when RGDS-DNA was removed at day 3 and cultured until day 7. (D,E) Cell area and aspect ratio as a function of culture time and RGDS-DNA presentation. Scale bar = 50 μm. (+) = RGDS on, (-) = RGDS off, T = experiment terminated. * = $p < 0.05$, ** = $p < 0.01$.

3.5 Troubleshooting

Possible problems and their solutions are listed in **Table 3.2**.

Table 3.2: Troubleshooting.

Step #	Problem	Causes	Suggestions
3.3.11	Hydrogel does not crosslink	Not using I2959	Make new batch with I2959.
3.3.11	Hydrogel partially crosslinks	1. DTT concentration is incorrect or too low	1. Make new batch of DTT and confirm DTT concentration is based on consuming at least 20% of the available norbornene groups. If still experiencing, refer to #2.
		2. The pH is too low	2. Dissolve NorHA in DI water and adjust to pH 7.
3.3.11	Hydrogel crosslinks without UV exposure	The pH is too low	Dissolve NorHA in DI water and adjust to pH 7.
3.3.11	Hydrogels appear fibrous	1. NorHA was partially dissolved	1. Vortex sample until fully dissolved. If still present, refer to #2.
		2. NorHA was lyophilized too long	2. Dissolve NorHA in DI water and adjust to pH 7.
3.3.12	No fluorescence after adding cB strand	1. No S DNA on surface due to the formation of disulfide bonds between DNA strands	1. Add TCEP to S DNA solution to break disulfide bonds.
		2. cB strand is not complementary	2. Check DNA sequence and (5'-3') directionality of S and cB strands.
		3. Fluorophore is photobleaching	3. Keep cB protected from light by covering with foil.
3.3.12	Fluorescence remains after adding cD strand	cD strand is not complementary	Check DNA sequence and (5'-3') directionality of cB and cD strands.
3.3.12	Fluorescence on control samples	Non-specific binding	Increase washing time and/or number of washes.

3.6 Conclusions

DNA nanotechnology has grown significantly over the past 40 years with research groups steadily developing new applications.[35,57–63] Due to the highly programmable nature of DNA, this work utilized ssDNA to incorporate fully reversible, temporal control of biomolecule presentation with a spatially controlled, photoresponsive hydrogel platform. A high norbornene functionalization was necessary for the uniform distribution of two biomolecule signals. To test the precise temporal control of DNA, complementary strands were able to add (cB) and remove (cD) the biomolecule signal.

DNA provides the additional benefit that only one bioconjugation strategy is necessary for each biomolecule, yielding a highly modular toolkit for attaching a variety of biological signals. This modular platform provides orthogonality to spatiotemporal and independent control of multiple biomolecules when using different DNA sequences and was demonstrated by creating a crosshatch pattern with S1 plus cB1 and S2 plus cB2 strands, where the addition and removal of cB1 or cB2 with cD1 or cD2, respectively, did not affect the control of the other biomolecule. Future work will utilize this *in vitro* platform to evaluate the relationship between cell-cell and cell-matrix adhesion motifs on osteogenesis as a function of spatiotemporal presentation. The reversible, DNA-NorHA biomaterial platform developed here has broad applications as an *in vitro* model system to understand the complex spatiotemporal relationship between biomolecule signaling and cell behavior. An improved understanding of these relationships would transform the design of drug delivery systems, disease modeling, tissue engineering, and others.

CHAPTER 4

TEMPORALLY PROBING THE EFFECTS OF CELL ADHESION MOTIFS IN COMBINATION WITH OSTEOGENIC GROWTH PEPTIDE ON OSTEOGENESIS

4.1 Introduction

Bone has three stages of osteogenic differentiation of mesenchymal stromal cells (MSCs).[81–85] In the first stage there is an increase in the number of cells, which occurs between days 1 to 4. The second stage can be seen from days 5 to 14, which involves early cell differentiation, and is typically characterized via alkaline phosphatase (ALP) expression. In the final stage, cells express high levels of osteopontin and osteocalcin followed by deposition of calcium and phosphate from days 14 to 28 (**Figure 4.1**).[82–85] The first two stages are of particular interest because cell adhesion molecules (CAMs) have been shown to have biological significance during these early stages of bone regeneration.[66,86–89]

CAMs are a subset of cell surface proteins that play a crucial role in regulating cell behavior and function. Two classes of CAMs are of specific interest: integrins and cadherins. Integrins have a high affinity for many ECM proteins (e.g. collagen,[90–93] fibronectin,[90–93] laminin[90–93]) and they facilitate cell-matrix interactions. These interactions are important for adhesion, migration, and differentiation. Cadherins form adherens junctions which mediate cell-cell interactions by binding to cadherins on nearby cells. These interactions are vital for regulating tissue morphogenesis and homeostasis.[94,95] The presentation of ECM proteins in combination with growth factors has been shown to dramatically improve growth factor efficacy.[96–99] However, far less is

known about the temporal dependence of these signals and their interactions with other biomolecular signals.

In this chapter, three different peptides were used to explore how the temporal presentation of these peptides affects early osteogenic differentiation by using the platform developed in Chapter 3. The peptides used were: 1) the fibronectin-derived peptide RGDS; 2) the N-cadherin mimetic peptide HAVDI; and 3) osteogenic growth peptide (OGP). RGDS is a cell-matrix adhesion peptide which allowed MSCs to adhere to the NorHA hydrogel surface.[90–93] HAVDI is a cell-cell adhesion peptide which was important for stabilizing new tissue development by forming adherens junctions and promoting intracellular signaling.[67] Lastly, OGP is a naturally occurring growth factor and osteoinductive peptide which was used to promote osteogenesis.[100–102] I hypothesized that the use of these adhesion peptides in combination with OGP would dramatically enhance or otherwise influence osteogenic differentiation. There was a particular interest to understand the role of N-cadherins during osteogenesis, since some studies have shown that it may be important at earlier time points during the differentiation process.[66,67]

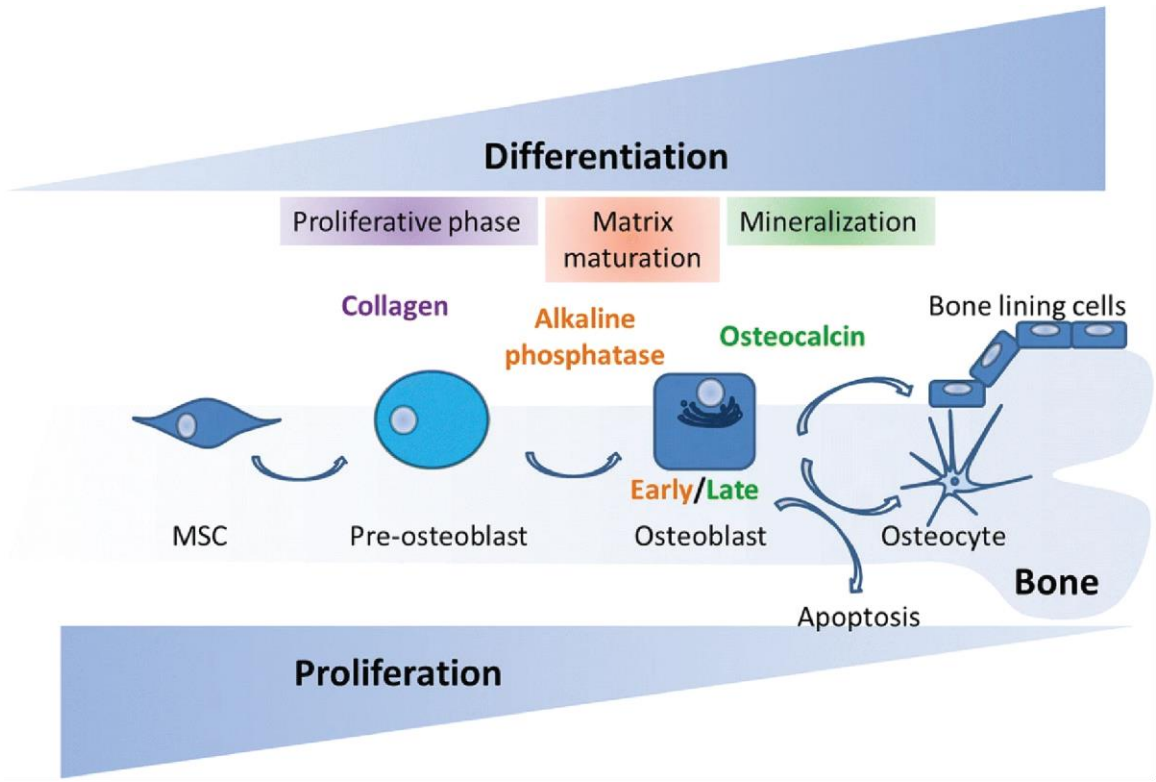

Figure 4.1: Schematic of the three stages of osteogenic differentiation. MSCs proliferate and have high levels of collagen production during the initial stage. As MSCs commit to osteoblasts, proliferation decreases while alkaline phosphatase secretion increases during the matrix maturation stage. Lastly, as osteoblasts mature, osteocalcin secretion increases during the mineralization stage.[85]

4.2 Materials and Methods

4.2.1 Norbornene Modified Hyaluronic Acid (NorHA) Synthesis

A two-step protocol was performed to synthesize norbornene-functionalized hyaluronic acid.[19,20] Firstly, hyaluronic acid-tetrabutylammonium (HA-TBA) salt was synthesized by exchanging the sodium salt of HA (Lifecore, 60-90 kDa) via acidic ion exchange with Dowex 50W×4 resin (50-100 mesh) and neutralized with 0.2 M tetrabutylammonium hydroxide (TBA-OH). The resin was added to 1% sodium hyaluronate in deionized (DI) water and stirred for 4 hours at room temperature. Then,

the solution was filtered and neutralized with TBA-OH to a pH of 7.02 to 7.05. Next, HA-TBA was frozen, lyophilized, and analyzed by ^{1}H NMR (Bruker Avance NEO 500 MHz). Secondly, NorHA was synthesized by combining HA-TBA and 5-norbornene-2-methylamine (Nor) in an oven-dried round bottom flask. The flask was sealed and purged with nitrogen gas for 10 minutes. Anhydrous dimethyl sulfoxide (DMSO) was cannulated into the sealed flask until the HA-TBA and Nor were completely dissolved yielding approximately a 2% solution. (Benzotriazole-1-yloxy)tris(dimethylamino) phosphonium hexafluorophosphate (BOP) was placed in a smaller oven-dried round bottom flask, sealed, and purged with nitrogen. BOP was dissolved in 25 mL of DMSO before being cannulated into the HA-TBA and Nor solution. The solution was left to react for 2 hours at room temperature with stirring and afterwards underwent extensive dialysis (Fisher Scientific, 6-8 kDa MWCO) against DI water at room temperature until purified. The resulting NorHA solution was frozen, lyophilized, and analyzed by ^{1}H NMR to ensure complete TBA removal and determine the norbornene functionalization percent.

4.2.2 Thiolation of Glass Slides

Glass slides were modified using Sylgard® 184 mixed with (3-mercaptopropyl)trimethoxysilane (MPTS). Sylgard® 184 components were mixed at a 10:1 (base:catalyst) ratio with 10 µL of MPTS per 1 g of Sylgard®. Using a spatula, glass slides were coated in a thin layer and then baked at 125 °C for 1 hour. Modified slides were sequentially washed in dichloromethane, ethanol, and DI water to remove any uncured Sylgard®. Samples were dried and stored under vacuum until used.

4.2.3 NorHA Hydrogel Formation

NorHA hydrogels were formed by dissolving NorHA in 0.05% Irgacure 2959 (I2959) photoinitiator in phosphate buffered saline (PBS) and crosslinked with non-degradable DL-dithiothreitol (DTT). The thiols on DTT allow for rapid crosslinking via step growth photopolymerization with the norbornene functional groups. DTT was added in a molar ratio of 0.2:1 thiol to norbornene leaving 80% of the original norbornene groups available for tethering DNA. The hydrogel solution was pipetted into cylindrical silicone wells, covered with a thiolated glass slide and photopolymerized using a curing lamp (OmniCure S1500, Excelitas Technologies) with an external UV filter (320-390 nm) at an intensity of 10 mW/cm^2 for 5 minutes. All hydrogels were synthesized to yield a final polymer concentration of 4%.

4.2.4 Peptide Synthesis

All peptides (**Table 4.1**) were synthesized using microwave assisted solid phase synthesis on a CEM Liberty Blue at a 0.1 mmol scale using a Rink Amide AM resin (0.57 mmol/g). Standard FMOC chemistry was applied, briefly described: 20% piperidine solution was used to deprotect, 0.2 M amino acids were activated and coupled over 4 minutes with 0.5 M diisopropylcarbamide and 1 M oxyma with 0.1 M diisopryopylethylamine. Peptides were cleaved using a mixture of trifluoroacetic acid (TFA), 2,2'-(ethylenedioxy) diethanethiol (DODT), triisopropylsilane (TIPS), and water in ratios of 90:5:2.5:2.5, respectively, over 4 hours at room temperature. Crude peptides were precipitated using cold diethyl ether and purified on a Waters HPLC with a Phenomenex C18 column and water/acetonitrile with 0.1% TFA. A linear gradient of 0 to

80% acetonitrile over 60 minutes was applied and peaks observed at 230 nm were collected and analyzed using MALDI TOF MS (Bruker Microflex LRF) employing α-cyano-4-hydroxycinnamic acid as the matrix. Pure fractions were consolidated and lyophilized and stored at -20 °C until further use.

Table 4.1: Peptide sequences for RGDS, HAVDI, and OGP. Z represents azidolysine.

Name	Peptide Sequence
RGDS	ZGYGRGDSPG
HAVDI	ZGGIDVAH
OGP	ZGGCGALKRQGRTLYGFGG

4.2.5 Peptide-DNA Conjugate Synthesis

All 5' amine modified oligonucleotides (single-stranded DNA, ssDNA) were purchased from Integrated DNA Technologies (Coralville, Iowa, **Table 4.2**) and resuspended in 10 mM PBS (pH 7.5) to 500 µM. Ten µL of 100 mM NHS-Sulfo-DBCO ester (Sigma) was added and allowed to react for 3 hours after which another aliquot of DBCO was added. The DBCO modified oligonucleotide was purified using an Agilent 1220 Infinity HPLC with a Zorbax Eclipse XDB C18 column. Using 50 mM triethylammonium acetate and 100% methanol, a linear gradient of 0-80% methanol was generated over 45 minutes. Both 260 and 309 nm were observed and peaks that were observed over a 200 mAU threshold were collected and concentrated using a 3 kDa MWCO spin filter. The fraction that contained the peak that displayed both an absorbance at 260 nm for the oligonucleotide and 309 nm for the DBCO was mixed with the corresponding azidolysine labeled peptide in 10 mM PBS at a 1:4 molar ratio and was allowed to react overnight at room temperature. The peptide-DNA conjugate was then purified using the same HPLC method as the DBCO modified oligonucleotide and the

desired peak was identified using MALDI TOF MS with 6-aza-2-thiothymine as a matrix.

Table 4.2: ssDNA sequences for surface (S), complementary biomolecule (cB), and complementary displacement (cD) strands for HAVDI (1), RGDS (2), and OGP (3) addition and removal.

Name	DNA Sequence (5'→3')
HAVDI	
S1	HS-AGTTTCGTCCAACGCTCAAGAAC
cB1	NH2-TTTTTGTTCTTGAGCGTTG-Fluorescein
cD1	CAACGCTCCAGAACAAAAA
RGDS	
S2	HS-TCATCTACGTTGAACCTGCCACA
cB2	NH2-AAAAATGTGGCAGGTTCAA-Rhodamine
cD2	TTGAACCTGCCACATTTTT
OGP	
S3	HS-GACCTCCAGCTATGCCGATGCTG
cB3	NH2-ATATATGTGGCAGGTTCAG
cD3	CTGAACCTGCCACATATAT

4.2.6 DNA Conjugation to NorHA Hydrogels

All ssDNA was purchased from Integrated DNA Technologies (Coralville, Iowa, **Table 4.3**). Different ssDNA sequences were used to assess DNA specificity: surface (S), complementary biomolecule with toehold region (cB), complementary displacement with toehold region (cD), mismatched biomolecule (mB), and mismatched displacement (mD) strands with (1) fluorescein and (2) rhodamine attached to the biomolecule strands. To tether S DNA strands to the hydrogel surface, 50 μM S DNA in 0.05% I2959 was added to the hydrogel surface for 5 minutes and exposed to UV for 60 seconds at 10 mW/cm^2. Unconjugated DNA was removed by washing with PBS. To verify successful tethering, cB strands containing a toehold region were added at a concentration of 50 μM for 5

minutes, washed with PBS for 4 hours, and imaged using a fluorescence microscope (Leica DMI6000 B). To demonstrate temporal control, cD DNA strands fully complementary to cB were added at a concentration of 100 μM for 30 minutes to remove cB via toehold-mediated strand displacement, washed with PBS for 4 hours, and imaged. mB and mD DNA strands as well as no S DNA bound to the surface were used as controls.

Table 4.3: ssDNA sequences for surface (S), complementary biomolecule (cB), complementary displacement (cD), mismatched biomolecule (mB), and mismatched displacement (mD) strands for (1) fluorescein and (2) rhodamine.

Name	DNA Sequence (5'→3')
Fluorescein	
S1	HS-AGTTTCGTCCAACGCTCAAGAAC
cB1	Fluorescein-TTTTTGTTCTTGAGCGTTG
cD1	CAACGCTCCAGAACAAAAA
Rhodamine	
S2	HS-TCATCTACGTTGAACCTGCCACA
cB2	Rhodamine-AAAAATGTGGCAGGTTCAA
cD2	TTGAACCTGCCACATTTTT
mB2	Rhodamine-AAAAAATCTATGTGCCGAT
mD2	AGCTTAGCAGATCTCCCCC

4.2.7 Peptide-DNA Hydrogels for Cell Culture

All hydrogels were soaked in ethanol for 30 minutes, washed 3-5x for 10 minutes each in sterile PBS, and stored in PBS in a biosafety cabinet until used. For RGDS studies, hydrogels were soaked in 50 or 100 μM of S2 in 0.05% I2959 for 5 minutes, exposed to UV light for 60 seconds at 10 mW/cm^2, and washed in PBS. Then, 50 or 100 μM of RGDS-DNA was added to the surface. For OGP studies, hydrogels were soaked in 0.1, 1, or 10 nM of S3 in 0.05% I2959 for 5 minutes, exposed to UV light for 60 seconds at 10 mW/cm^2, and washed in PBS. Then, 0.1, 1, or 10 nM of OGP-DNA was added to

the surface at day 0 (D0-7 and D0-14) or day 7 (D7-14). OGP-DNA was removed via cD3 on day 7 (D0-7). For combination studies, hydrogels were soaked in 100 μM of S1 and/or S2 and 0.1 nM of S3 in 0.05% I2959 for 5 minutes, exposed to UV for 60 seconds at 10 mW/cm^2, and washed in PBS. HAVDI-DNA and/or RGDS-DNA were added to the surface at 100 μM at day 0, day 3, or day 7. OGP-DNA was added at 0.1 nM on day 7. HAVDI-DNA or RGDS-DNA were removed at day 3 or day 7 via cD1 or cD2, respectively. Samples with no peptides served as a negative control while OGP-DNA only (D7-14) served as a positive control.

4.2.8 Measure-iT Thiol Assay

Serial dilutions of RGDS ranging from 0-2 mM were prepared in 0.05% I2959 in PBS. Each solution was added dropwise to the surface of the hydrogels (5 μL) and immediately exposed to UV light for 60 seconds at 10 mW/cm^2. The liquid layer was extracted from each hydrogel, added to a black 96-well plate, and the remaining thiols were measured using the thiol assay kit per manufacturer's protocol. All samples were measured in triplicate.

4.2.9 Mechanical Testing

Bulk uniaxial compression tests were performed on NorHA hydrogels using a mechanical testing system (Instron 5943, 50 N load cell). Hydrogel compressive modulus was determined for three different groups with and without tethered DNA (no DNA; S1 and S2; S1-cB1 and S2-cB2; n = 6). Cylindrical hydrogels (diameter: 4.8 mm, height: 4.3 mm) were compressed at a strain rate of 20% per min for 60 seconds. The stress versus

strain curve was plotted and the initial linear region of the curve (0-2.5% strain) was used to calculate the compressive modulus.

4.2.10 Cell Culture of hMSCs

Human mesenchymal stromal cells (hMSCs) (Lonza) were cultured and passaged using standard cell culture protocols.[103,104] For cell morphology studies, hydrogels were placed into an 8-well plate and hMSCs were seeded at 5,000 cells/cm^2 in standard growth media (16% fetal bovine serum, 1% penicillin/streptomycin, 1% L-glutamine). Media was changed every 2-3 days. For osteogenic differentiation studies, hydrogels were made in 96-well plates and hMSCs were seeded at 25,000 cells/cm^2 in standard growth media for 24 hours. Then, cells were cultured in osteogenic differentiation media (StemXVivo) for the remainder of the study. Media was changed every 3-4 days.

4.2.11 Cell Morphology Staining

Samples were prepared for immunofluorescence by first fixing the cells in 4% PFA for 30-45 minutes, permeabilizing in 0.1% Triton X-100 for 15 minutes and blocking non-specific binding in 5% BSA for 1 hour at room temperature. Hydrogels were then incubated with either fluorescein or rhodamine phalloidin (actin stain, 1 µM concentration, Invitrogen) in 2.5% BSA at room temperature for 1 hour to determine cell area. Then, hydrogels were incubated with DAPI (nucleus stain, 300 nM concentration, Invitrogen) in 2.5% BSA at room temperature for 10 minutes to determine cell number. Hydrogels were rinsed 3x for 10 minutes each and stored at 4 °C in the dark until

imaging. Fluorescent images were acquired using an Olympus BX63 microscope and analyzed using ImageJ.

4.2.12 Alkaline Phosphatase Activity

Cell culture media was removed and cells were washed in PBS twice. Then, cells were lysed using a radio-immunoprecipitation assay (RIPA) buffer. RIPA buffer (200 µL) was added to each sample and incubated at 4 °C for 20 minutes. Samples went through two freeze/thaw cycles at -80 °C before clarifying the lysate by centrifugation at 8,000×g for 10 minutes at 4 °C. The supernatant was transferred to a centrifuge tube on ice for further analysis. Cell number was determined using the PicoGreen DNA Kit (Molecular Probes). The manufacturer's guidelines were adjusted to perform the assay in a black 96-well plate. The 1-Step p-nitrophenyl phosphate (PNPP) assay (Thermo Fisher) was used to determine alkaline phosphatase (ALP) expression per manufacturer's protocol. In a 96-well plate, 100 µL of PNPP was added to 50 µL of cell supernatant per well. Samples were incubated at room temperature on a rocker plate for 15-30 minutes or until sufficient color developed. The reaction was stopped with 50 µL of 2 N NaOH and the absorbance was measured at 405 nm. ALP activity was normalized to DNA content from the PicoGreen assay.

4.2.13 Statistical Analysis

All values were reported as mean ± standard deviation for at least three independent samples. Statistical significance was determined using a one-way or two-way analysis of variance (ANOVA) followed by a Tukey's multiple comparisons test

with a 95% confidence interval. Significance was indicated by *, **, ***, or **** corresponding to $p < 0.05$, 0.01, 0.001, or 0.0001, respectively. Figures were simplified by only showing relevant statistical significance.

4.3 Results and Discussion

4.3.1 DNA Linkages Provide Reversibility and Orthogonality

The use of reversible DNA linkages to temporally control biomolecule presentation via toehold-mediated strand displacement was confirmed. Five distinct ssDNA sequences were used to assess the high specificity of DNA and how it can be used as a reversible linker: surface (S), complementary biomolecule with toehold region (cB; fluorophores were used as a model molecule and for visualization), complementary displacement with toehold region (cD), mismatched biomolecule (mB), and mismatched displacement (mD) strands. DNA sequences for each strand are in **Table 4.3**. The S strand was permanently bound to the hydrogel surface via radical-mediated photoconjugation of a thiol group at the end of the S strand to a norbornene group within HA (**Figure 4.2A**). When cB was introduced, a DNA duplex forms between cB and S via DNA hybridization. A short, single-stranded "toehold" region was added to the cB and cD strands to promote toehold-mediated strand displacement, where cD outcompetes S via branched migration to remove cB from the hydrogel surface. Controls for this system were mB and mD strands, as well as hydrogels without S on the surface. A schematic of these outcomes is in **Figure 4.2B-E**.

When mB was added to the surface there was no fluorescent signal; however, a fluorescent signal was observed when cB was added. When mD was added, cB was not

removed from the surface evidenced by the remaining fluorescent signal. But, when cD was added, cB was removed resulting in a 98% reduction of fluorescent signal (**Figure 4.3A**). Fluorescent images demonstrating these changes are in **Figure 4.3A, inset**. This demonstrates the importance of S, cB and cD strands being complementary to each other. Samples with no S had no fluorescent signal following the addition of cB, indicating that S needs to be tethered on the surface for cB binding to occur. Additionally, this result suggested that there was no non-specific binding of cB to the NorHA hydrogel. The cB and cD strands were then used to determine if DNA linkages could be used to reversibly control fluorescent signaling over multiple cycles. In **Figure 4.3B**, a fluorescent signal was added via cB (signal "ON") and removed via cD (signal "OFF") over five full cycles while maintaining a constant fluorescent intensity for the signal "ON" state.

To demonstrate the benefit of using DNA, two different sets of DNA sequences were designed to explore the precise and independent control of each set of strands (**Table 4.3**). Initially, the hydrogel was photopatterned with S1 and S2 over the entire surface and fluorescence was observed when both cB1 and cB2 strands were presented (**Figure 4.3C**). When cD2 was added, cB2 was removed leaving only cB1 on the surface (**Figure 4.3D**). Lastly, cD1 and cB2 were added simultaneously, removing cB1 and leaving only cB2 present on the surface; this result indicates that control of one signal had no effect on the control of the other (**Figure 4.3E**). Overall, these results demonstrate that it is necessary for the ssDNA strands to be complementary for addition and removal of the biomolecule strand and due to this specificity DNA provides full reversibility and complete orthogonality when working with multiple signals.

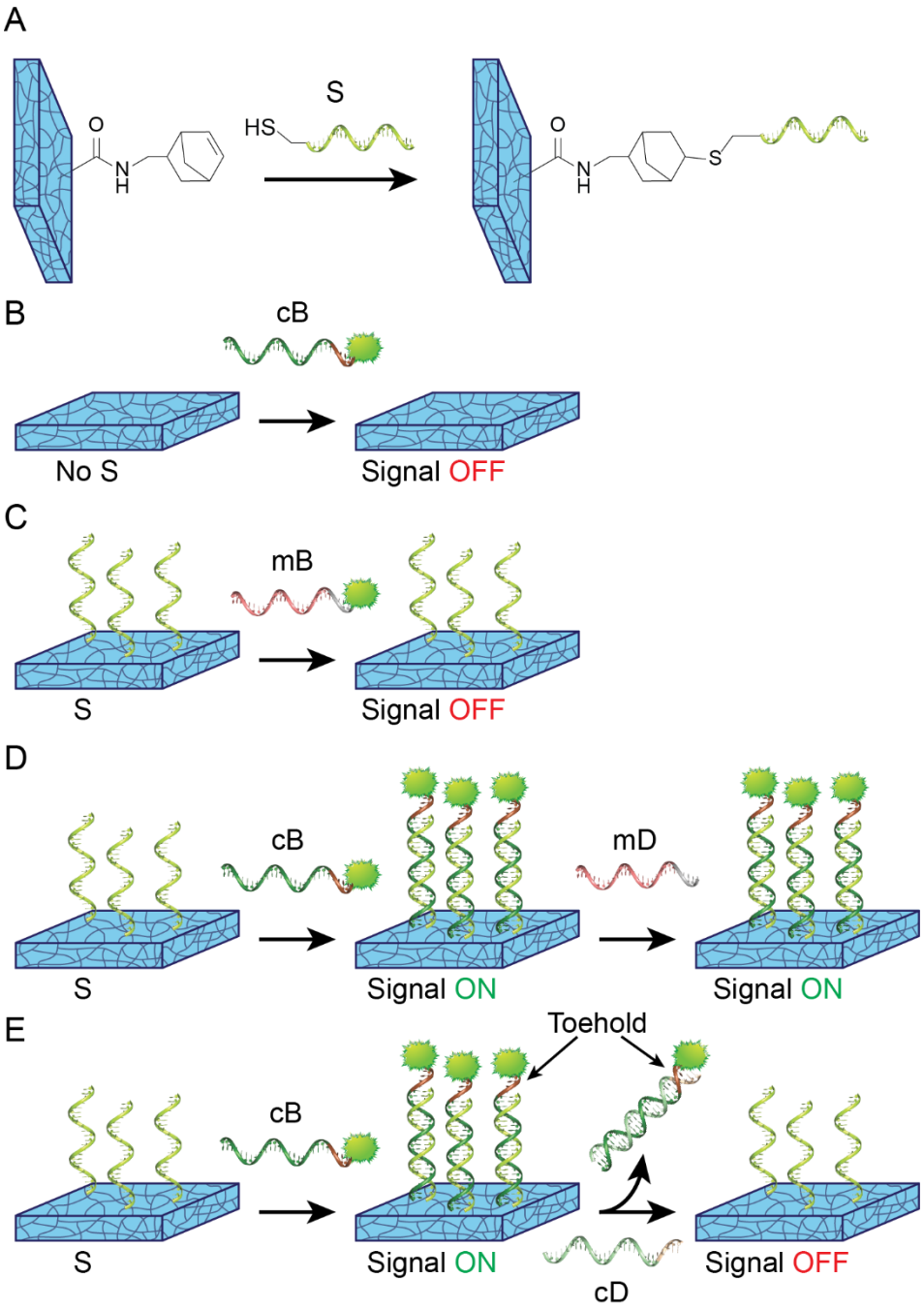

Figure 4.2: Schematic of complementary and mismatched ssDNA binding. (A) NorHA hydrogel pre- and post-modification with the S strand via radical-mediated coupling. (B) No S bound to NorHA results in no signal when cB is added. (C) S bound to NorHA with mB added results in no signal. (D,E) S bound to NorHA with cB added results in the signal being "ON". When removing cB with (D) mD the signal remains "ON" while (E) cD the signal is turned "OFF."

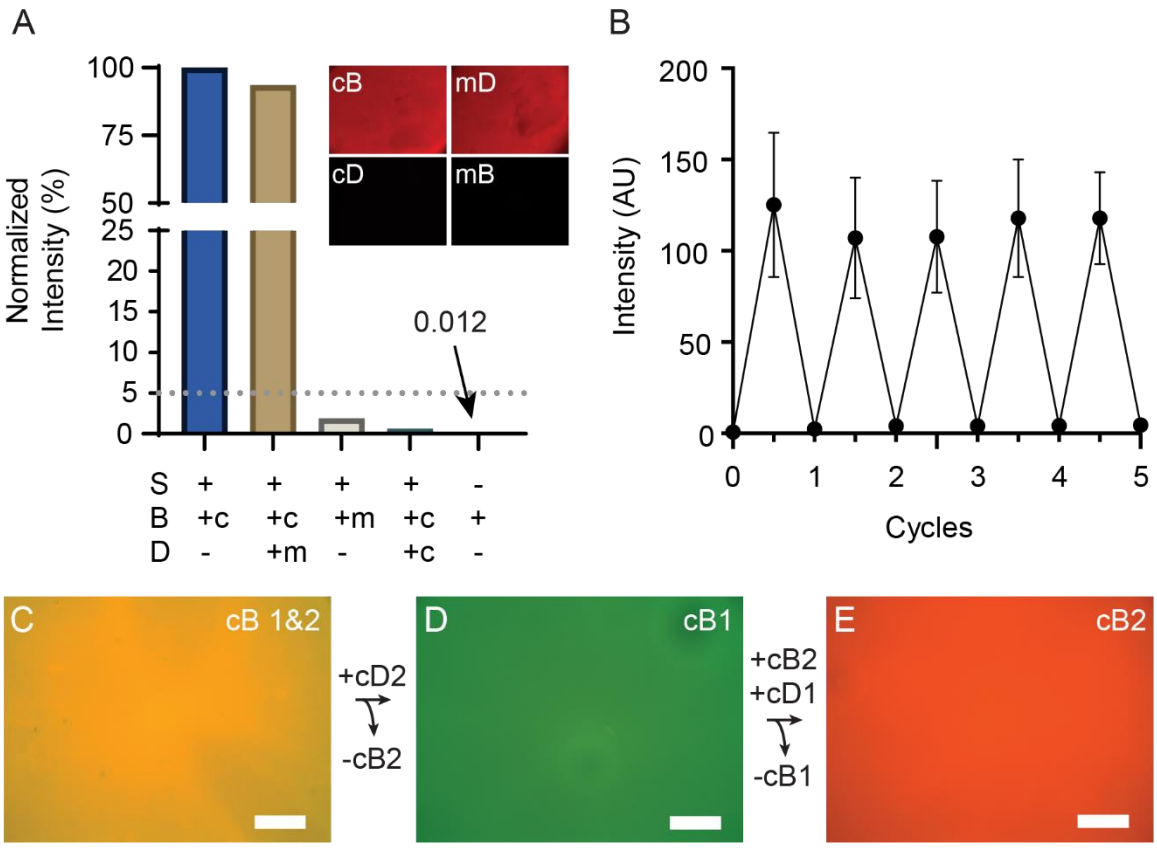

Figure 4.3: DNA handles support full reversibility and orthogonal control of multiple biomolecule signals. (A) To demonstrate precise temporal control, cB, cD, mB, and mD ssDNA strands were added to a hydrogel platform. The controls mC, mD and no S indicate no non-specific binding occurs and that cB and cD are necessary for addition and removal of the fluorescent signal, respectively (inset). (B) cB and cD strands were alternatively added over five full cycles revealing that DNA handles can be used to reversibly control biomolecule signal presentation with no degradation of signal intensity (n=4). (C-E) To demonstrate orthogonal control, (C) S1 plus cB1 and S2 plus cB2 were added to the surface. (D) When cB2 was removed via cD2 addition, only cB1 remained. (E) When cD1 and cB2 were added simultaneously, cB1 was removed leaving only cB2 on the surface and demonstrating independent control of each strand. Scale bar = 200 μm.

4.3.2 Biomolecule Conjugation was Efficient and Does Not Impact Mechanical Properties

Cell morphology and differentiation can be influenced by both the presence of cell adhesion molecules and surface stiffness.[105–108] Before performing cell experiments, it was critical to determine the precise amount of peptide successfully conjugated to the

hydrogel surface, and that this modification did not affect hydrogel stiffness. First, RGDS solutions at concentrations ranging from 0-2000 μM were added to the hydrogel surface and tethered via UV light exposure. The RGDS solution was collected, and a thiol assay was used to detect any residual, unreacted RGDS in solution. These values were then subtracted from the original concentration to determine tethered RGDS. At each concentration, very low amount of RGDS remained verifying that approximately all of the RGDS was tethered to the surface (**Figure 4.4A**).

Next, bulk compression tests were performed to determine the hydrogel's elastic compressive modulus, and to verify that the addition of biomolecules via DNA linkages does not further crosslink the hydrogel or otherwise impact hydrogel mechanical properties. Three experimental groups were prepared: no S strand on the surface (hydrogel only control), two different S strands (S1 and S2), and two different cB strands (cB1 and cB2) bound to their respective S strands. All hydrogel groups had an elastic compressive modulus of approximately 15 kPa with no statistical differences between groups, indicating the hydrogel does not crosslink during S DNA photoconjugation and the presence of DNA strands does not impact the bulk hydrogel mechanical properties (**Figure 4.4B**).

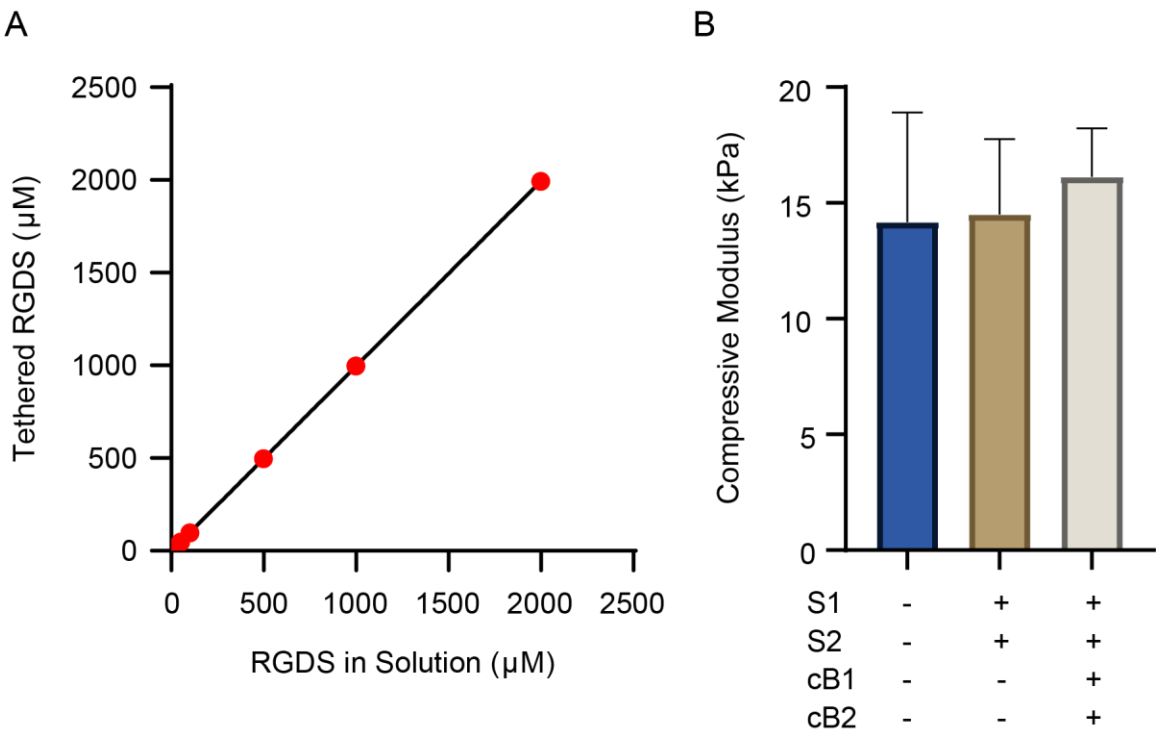

Figure 4.4: Biomolecule conjugation tethers at desired concentration and does not impact hydrogel compressive modulus. (A) Tethered RGD density on hydrogel surfaces as a function of RGD concentration in solution shows that approximately all of the RGD in solution is tethered to the surface post UV exposure. Linear regression: y = 0.9981x – 2.072. (B) Compression tests were performed on three different samples: hydrogel only, S 1&2, and S 1&2 with cB 1&2. There were no statistical differences (p > 0.05) between groups indicating that DNA does not further crosslink the hydrogels. (+) = "ON", (-) = "OFF".

4.3.3 Synthesis of HAVDI-, RGDS-, and OGP-DNA Conjugates

In order to perform the cell experiments, peptide-DNA conjugates were synthesized. ssDNA strands were purchased from Integrated DNA Technologies (**Table 4.2**) while all peptides were made in-house via solid-phase peptide synthesis (**Table 4.1**). The peptides incorporated an N-terminal azidolysine amino acid to enable copper-free click coupling to cyclooctyne-DNA (**Figure 4.5A**). The peptide-DNA conjugates were purified via reverse-phase high performance liquid chromatography (HPLC) and their

identity and purity verified by matrix-assisted laser desorption/ionization time-of-flight (MALDI-TOF) mass spectrometry. Possible discrepancies associated with the actual mass varying slightly from the expected mass could be trace amounts of salts (e.g. sodium, potassium, etc.), calibration errors, or differences in the DNA mass ordered versus actual DNA mass. However, the amount of error was not unexpected and within reason for determining peptide-DNA identity. MALDI-TOF spectra of RGDS-, HAVDI-, and OGP-DNA are shown in **Figure 4.5B-D**. Detailed protocols for peptide synthesis and peptide-DNA conjugation are in Chapter 3.

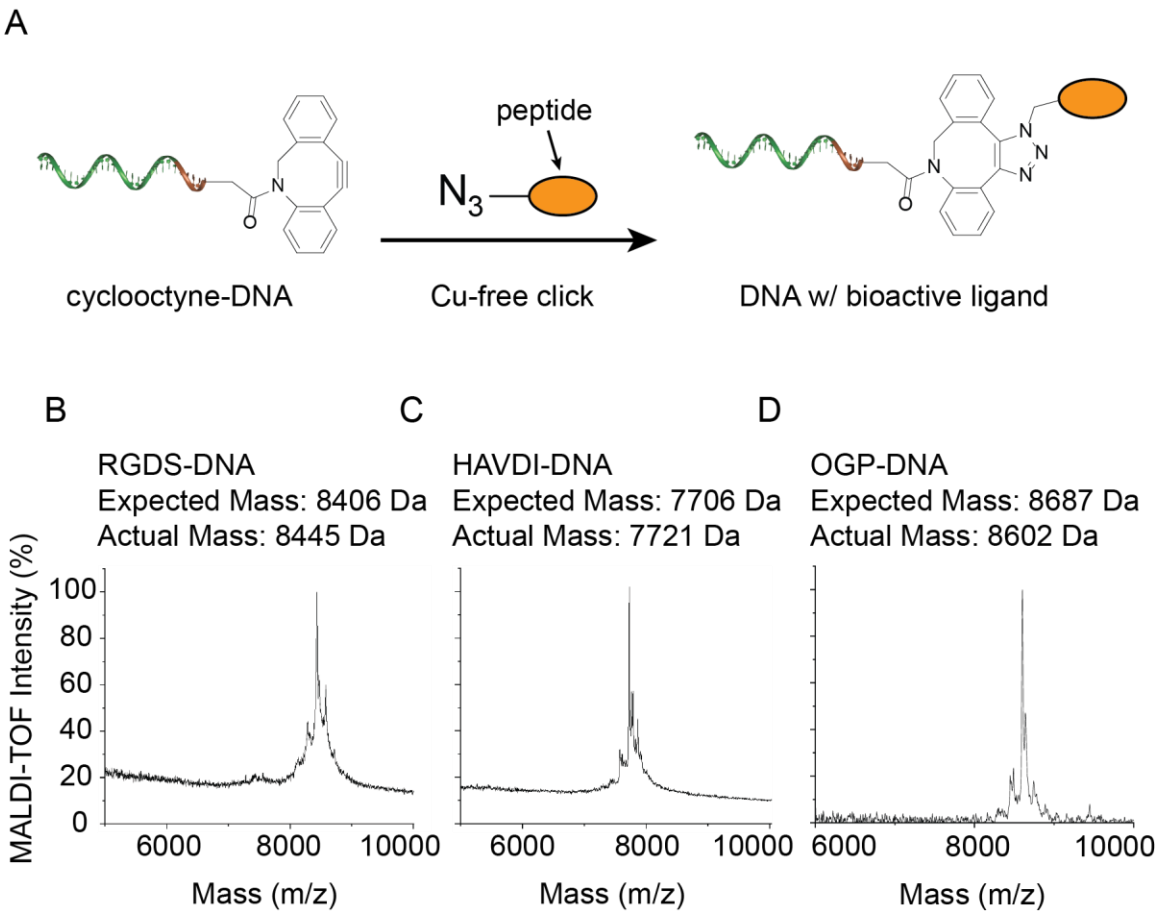

Figure 4.5: MALDI-TOF verifies peptide-DNA conjugate formation. (A) Peptide-DNA conjugates were formed by reacting an azidolysine with cyclooctyne via copper-free click chemistry. MALDI-TOF spectra verified the peptide-DNA conjugates of (B) RGDS, (C) HAVDI, and (D) OGP.

4.3.4 Medium-Range Concentrations of RGDS Are Adequate for Cell Spreading

Originally, peptides were labeled with a fluorophore; however, the fluorescence was quenched when attempting to conjugate the peptide to DNA. Therefore, fluorescently labeled DNA was used instead to visualize the cB DNA strands. Unfortunately, synthesizing fluorophore labeled DNA requires extra purification steps, resulting in low yields and high costs. To determine the optimal cell adhesion peptide concentration, surfaces were modified with RGDS peptides (without DNA) at various

concentrations ranging from 0 to 1000 μM with 0 and 1000 μM serving as negative and positive controls, respectively. Cells were cultured in growth media for 3 days, fixed in 4% paraformaldehyde, and stained with FITC-phalloidin (actin) and DAPI (nucleus) to determine cell area and cell number, respectively. The cell area at low (5 and 10 μM) and medium (50 and 100 μM) RGDS concentrations in comparison to the controls is in **Figure 4.6A**. An increase in cell spreading was observed as the RGDS concentration increased. Furthermore, cell spreading on RGDS and RGDS-DNA samples were comparable to each other at similar concentrations, indicating the presence of DNA does not impact RGDS bioactivity. Since the intermediate ("medium") RGDS concentrations demonstrated sufficient cell spreading, conserved the amount of DNA needed, experiments were performed at this range with RGDS-DNA at 50 and 100 μM being statistically significant ($p < 0.05$) when compared to no RGDS. Thus, all future experiments were performed using 100 μM concentrations for RGDS-DNA.

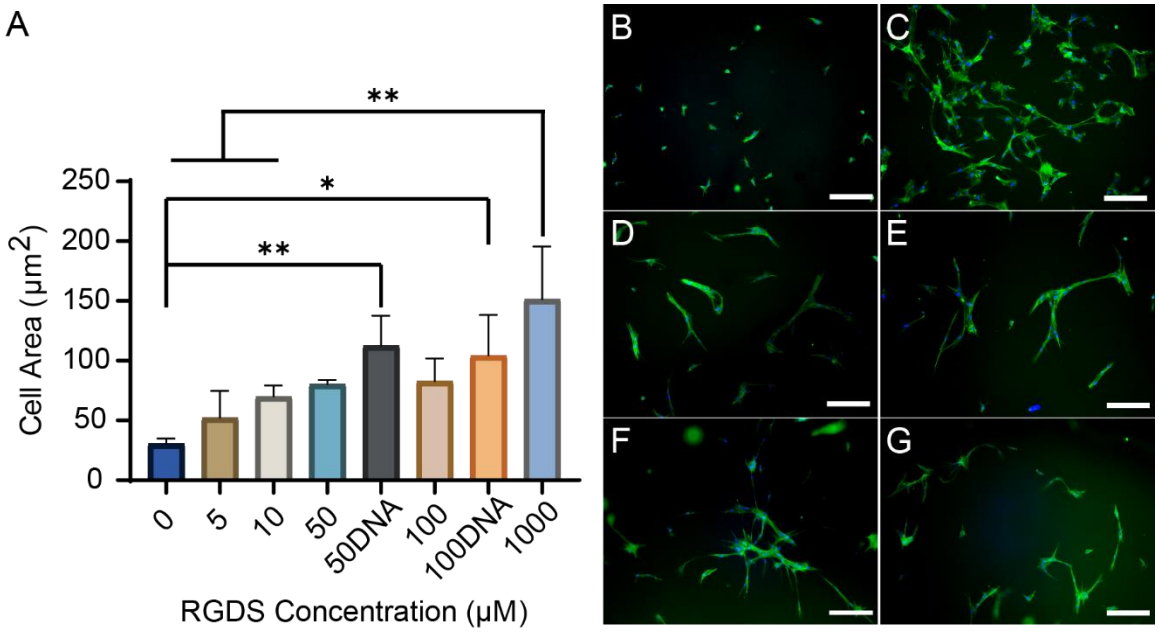

Figure 4.6: RGDS at higher concentrations increases cell spreading. Hydrogels were modified with varying concentrations of RGDS. (A) Surfaces bearing higher RGDS concentrations had more cell spreading compared to no RGDS. Images of the controls at (B) 0 μM RGDS reveal little to no cell spreading while cells were well spread at (C) 1000 μM RGDS. Images at (D) 50 and (E) 100 μM RGDS, as well as (F) 50 and (G) 100 μM RGDS-DNA show sufficient cell spreading compared to no RGDS (B). Scale bar = 200 μm.

4.3.5 HAVDI Increases Cell Spreading Without the Presence of RGDS

To determine optimal HAVDI concentration, hydrogels were made with no RGDS in the bulk hydrogel and the surfaces were modified with HAVDI (without DNA) at concentrations ranging from 0 to 1000 μM with the extreme values serving as negative and positive controls, respectively. Cells were cultured in growth media for 3 days, fixed in 4% paraformaldehyde, and stained with rhodamine-phalloidin (actin) and DAPI (nucleus) to determine cell area and cell number, respectively. The images in **Figure 4.7** display cell spreading at (A) 0, (B) 100, and (C) 1000 μM HAVDI. An increase in cell spreading was observed as HAVDI concentration increased. Since 100 μM HAVDI had

significant cell spreading ($p < 0.001$) compared to 0 μM HAVDI (**Figure 4.7D**), all future studies were performed at this concentration.

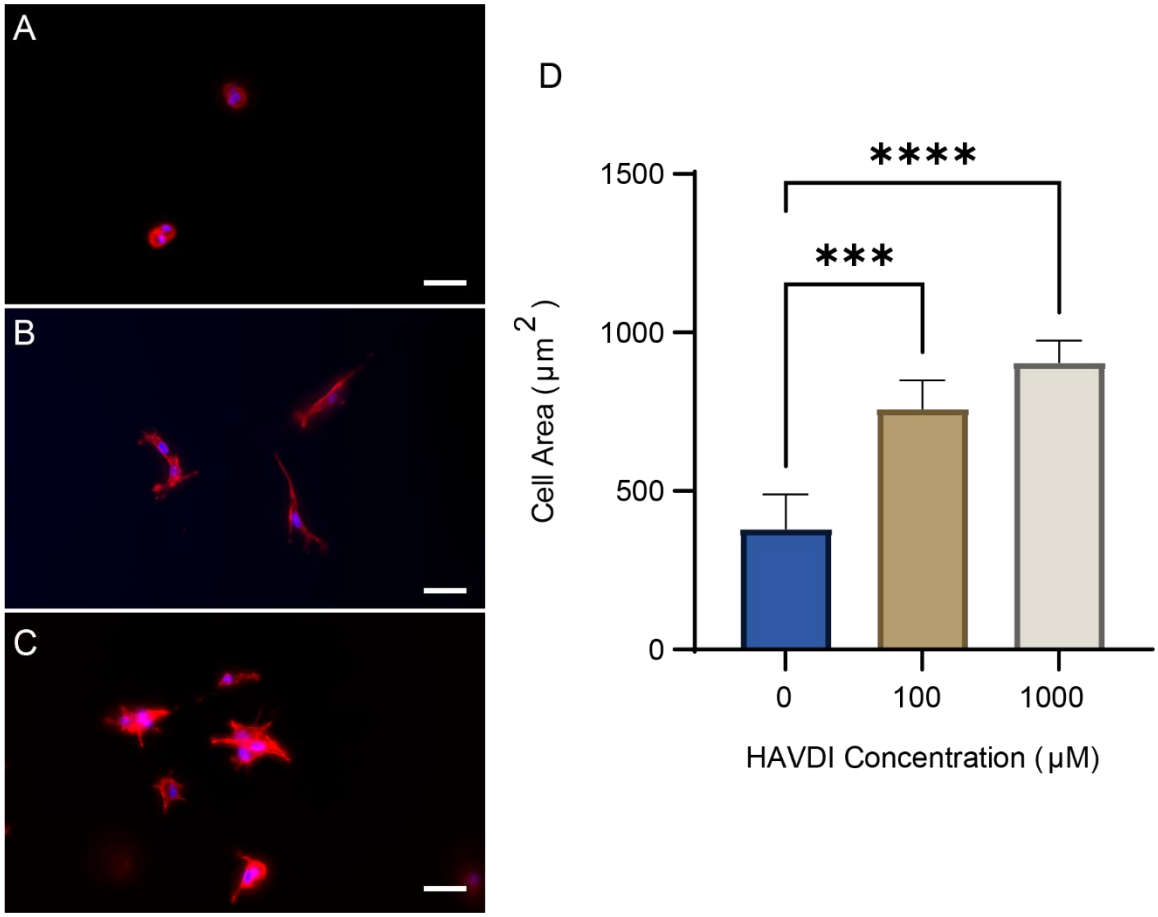

Figure 4.7: HAVDI at higher concentrations increases cell spreading. Hydrogels were modified with varying concentrations of HAVDI. Images of cell spreading at (A) 0, (B) 100, and (C) 1000 μM HAVDI. (D) Surfaces with higher HAVDI concentrations had more cell spreading compared to no HAVDI. Scale bar = 50 μm.

4.3.6 Temporal Presentation of HAVDI, RGDS, and OGP Affects Alkaline Phosphatase Activity

Previous research has reported that OGP concentrations between 1 pM and 10 nM stimulate bone formation and mineralization with an optimal concentration at 1 nM.[100] This was confirmed using tethered OGP peptide (t-OGP, without DNA) and OGP-DNA

at concentrations of 0.1, 1, and 10 nM. The temporal presentation of OGP-DNA was also studied to determine if constant (0-14 days, D0-14), early (0-7 days, D0-7), or late (7-14 days, D7-14) OGP presentation influenced ALP activity. At day 7, OGP-DNA was removed via cD3 for the D0-7 treatment group and OGP-DNA was added to the D7-14 treatment group. At day 14, all samples were lysed and analyzed. The controls confirmed that the presence of OGP significantly increases ALP activity ($p < 0.0001$) for all concentrations when compared to samples with no OGP. When comparing concentrations, 0.1 and 1 nM of OGP produced more ALP than 10 nM of OGP (**Figure 4.8A**). At 0.1 and 1 nM, OGP-DNA samples revealed that there was considerably more ALP expression when OGP was presented late (D7-14) compared to early (D0-7) presentation (**Figure 4.8B**). When constant (D0-14) OGP was present there was a slight increase in ALP activity compared to OGP presented early (D0-7); however, constant (D0-14) OGP presentation was slightly less active compared to when OGP was presented late (D7-14). When considering only the D7-14 samples, there was a higher expression of ALP at 0.1 and 1 nM than at 10 nM. Since there was no statistical difference between 0.1 and 1 nM at D7-14 and studies have shown higher cell proliferation at concentrations less than 1 nM,[100] all future studies with OGP-DNA were performed at 0.1 nM from D7-14.

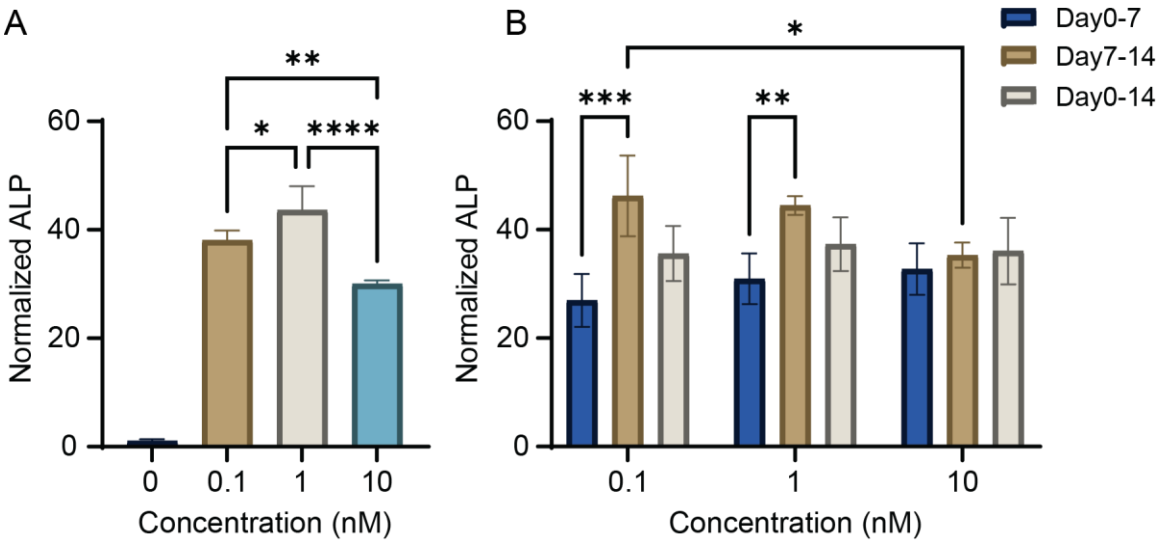

Figure 4.8: OGP present from day 7-14 has higher ALP expression compared to early or constant presentation. (A) Tethered OGP (t-OGP) at all concentrations resulted in significantly higher ALP expression compared to no OGP ($p < 0.0001$, not shown). ALP expression was highest at the intermediate t-OGP concentration. (B) OGP-DNA present late (D7-14) had higher ALP expression than when present early (D0-7) or constant (D0-14). There was no temporal effect at high OGP concentrations.

This was taken a step further by exploring how HAVDI and RGDS in combination with OGP affected ALP activity. All samples had their respective S DNA strands tethered to the surface and sterilized in ethanol. Samples with HAVDI- and/or RGDS-DNA present at day 0 were added before cell seeding. All samples were cultured for 14 days in osteogenic media. HAVDI- or RGDS-DNA were added at day 3 or day 7 for some samples and removed for others. OGP-DNA was added at day 7 for all experimental groups and the positive control (OGP-DNA only). After 14 days, all samples were lysed and analyzed.

Samples with static HAVDI-DNA or RGDS-DNA presentation for the entire 14 days had the same ALP activity as the negative control (no peptides) with the positive control (OGP-DNA) having significantly higher ALP activity (**Figure 4.9**). All dynamic

HAVDI-DNA and/or RGDS-DNA experimental groups that included OGP-DNA had high ALP expression (**Figure 4.10**), where all experimental groups were compared to the positive control. All dynamic samples where HAVDI-DNA was present from D0-3 were slightly higher than the positive control while samples without HAVDI-DNA from D0-3 were slightly less than the positive control, indicated by a dashed, red line in **Figure 4.10**. This could be due to the fact that cadherin mediated cell-cell interactions have been shown to have a large effect on directing MSC fate[109] or that cadherins can affect the Wnt/β-catenin pathway which regulates cell proliferation and differentiation in bone repair.[110–116] The sample with the highest ALP activity had HAVDI-DNA present from D0-7 and RGDS- and OGP-DNA present from D7-14. Samples where HAVDI- and RGDS-DNA were both present on D0-3 had high expression of ALP, but at a lower level than if only HAVDI-DNA was present on D0-3. This indicates that HAVDI is more important at earlier time points (D0-7) and may be necessary on D0-3 while RGDS is more important at later time points (D7-14) during early osteogenesis; however, further studies are necessary to verify this outcome.

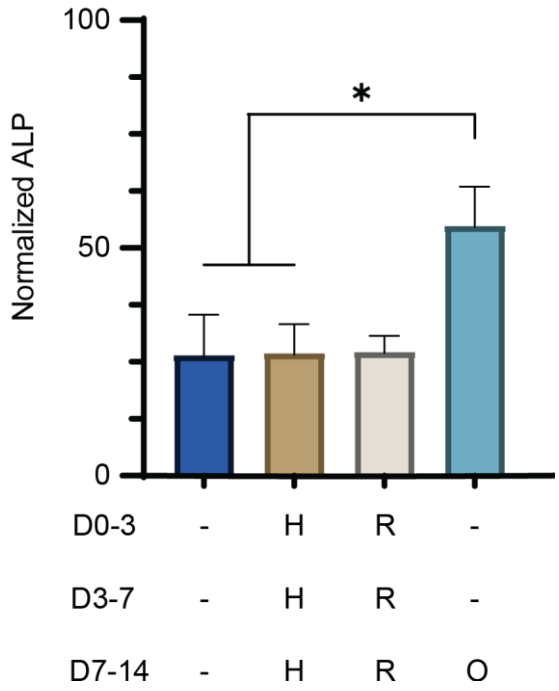

Figure 4.9: ALP expression remained low when HAVDI- and RGDS-DNA were presented from day 0-14. Samples with HAVDI- and RGDS-DNA presented from D0-14 were compared to the negative (hydrogel only) and positive (OGP-DNA presented from D7-14) controls. HAVDI- and RGDS-DNA groups showed minimal ALP expression similar to the negative control. (-) = no peptides, H = HAVDI "ON", R = RGDS "ON", O = OGP "ON".

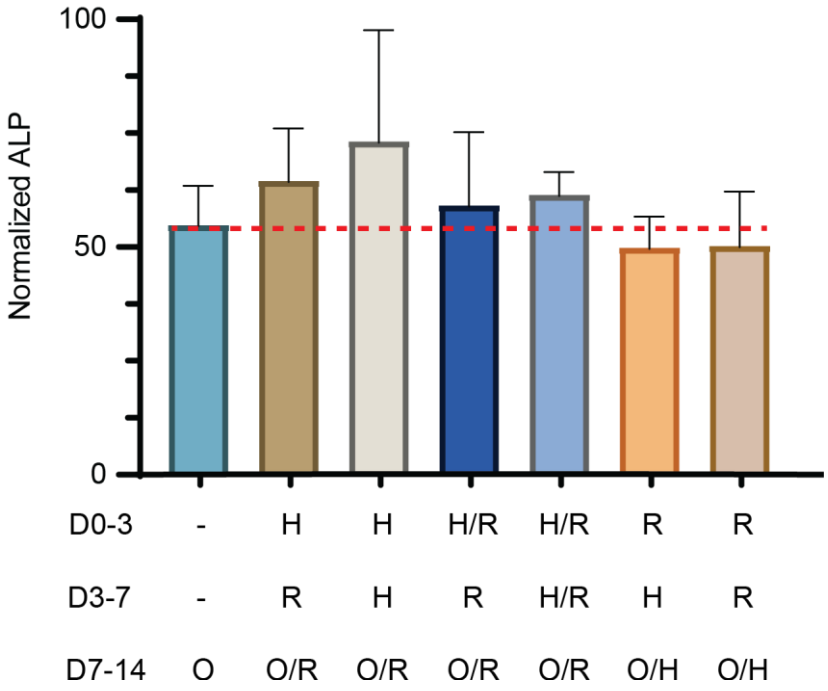

Figure 4.10: HAVDI-DNA presented on day 0-3 had slightly higher ALP expression compared to other dynamic groups. All experimental groups were compared to the positive control (OGP-DNA presented from D7-14), indicated by a dashed, red line. Samples where HAVDI-DNA was present on D0-3 had higher ALP expression while samples without HAVDI-DNA from D0-3 had lower ALP expression. (-) = no peptides, H = HAVDI "ON", R = RGDS "ON", O = OGP "ON".

4.4 Conclusions

Most dynamic approaches for controlling ligand presentation rely on either cleavable moieties[41–46] or UV-switchable groups,[33] which limits the number of biomolecules that can be controlled as well as the degree of independent control over each biomolecule. To circumvent this issue, ssDNA strands were used to control three peptide-DNA conjugates (HAVDI, RGDS, and OGP) reversibly and independently, which allowed us to probe the relationship between cell-cell and cell-matrix interactions during osteogenesis. A select set of combinations of these peptides at different time points revealed that cell-cell interactions are potentially more important at earlier time

points (specifically at D0-3), while cell-matrix interactions may be more important at time points after day 3; however future studies should be conducted to confirm this interaction. OGP was shown to have a higher effect on osteogenic differentiation when presented at day 7 than if the peptide was present from day 0. These results can be applied to develop scaffolds for *in vivo* experiments, where controlled delivery strategies can be employed to mimic the optimal presentation of these peptides. Overall, our system enables the investigation of the dynamics of cell signaling pathways at a level similar to the natural healing process and understanding these intricacies could have a transformative effect on the development of drug delivery systems, platforms for disease modeling, and tissue-engineered therapeutics.

CHAPTER 5

CONCLUSIONS AND FUTURE WORKS

5.1 Main Findings

There are five design parameters to consider when developing biomaterials that can mimic the dynamic signaling presentation of biomolecules. 1) The system needs to be fully reversible (over multiple cycles) to mimic the dynamic signaling cascades present during healing. 2) There must be spatial control to simulate the biochemical gradients found in natural tissue. 3) It needs to have orthogonality (independent control over multiple biomolecules) since numerous signals are presented at various times throughout the healing process. 4) It should only use a single conjugation scheme to provide simplicity and ease of use to the system. 5) And the platform must be easy to use so others can utilize this system to study their own research endeavors. There have only been a handful of groups to produce platforms that dynamically control biomolecule presentation, but they typically lack at least one of these five features. Through this work, I developed an *in vitro* platform that can spatially and temporally control multiple biomolecules using a single conjugation scheme.

To address these five parameters, DNA was combined with a photoresponsive norbornene-modified hyaluronic acid (NorHA) hydrogel. Since NorHA is photoresponsive, the system could spatially control biomolecule placement through the use of photomasks and a light source. The high specificity of DNA base pairs forming duplexes combined with toehold mediated displacement provided the system with

reversibility and orthogonality which was verified by independently cycling multiple biomolecules “ON” and “OFF” with spatiotemporal control over several cycles. Lastly, tethering DNA to NorHA required a single conjugation scheme which overall made the system easy to use.

Other key takeaways when developing this platform were optimizing NorHA functionalization and determining DNA sequence specificity, hydrogel stiffness, and DNA-NorHA conjugation efficacy. The functionalization of NorHA must be ~60% or greater for there to be enough norbornene groups to tether multiple signals post hydrogel formation. Further, the DNA strands must be complementary to each other for complete addition and removal of the biomolecule signal while the specificity of the DNA sequence can be tailored to orthogonally control multiple signals. Another main factor was confirming that the addition of DNA strands did not further crosslink the hydrogel or otherwise modify hydrogel mechanical properties since cell behavior can change with scaffold stiffness. Lastly, it was essential to verify the efficiency of the DNA conjugation onto the hydrogel surface and the corresponding DNA concentration. A thiol assay kit was used to detect unreacted RGDS peptides post UV light exposure which indicated approximately all RGDS peptides were successfully tethered to the hydrogel surface.

After developing this platform, it was used to explore the temporal role of cell adhesion motifs and osteogenic growth peptide (OGP) on the early stages of osteogenesis. The cell-matrix mimetic peptide RGDS and the cell-cell mimetic peptide HAVDI were studied individually to determine the optimal concentration necessary for bioactivity, assessed via cell spreading, while limiting the amount of DNA. Enhanced cell spreading occurred at 100 μM for both RGDS and HAVDI compared to no peptide

controls. OGP was also studied individually to determine two parameters: 1) the optimal concentration for bioactivity and 2) the optimal time range for OGP presentation, where both parameters were assessed using alkaline phosphatase (ALP) activity. Within the concentration range tested, lower concentrations of OGP, particularly 0.1 nM, exhibited the highest ALP activity. When exploring the temporal presentation of OGP, ALP expression was highest when OGP was present from day 7-14 and the lowest when OGP was present from day 0-7 indicating that OGP presentation is important at later time points during osteogenesis.

Lastly, RGDS, HAVDI, and OGP-DNA were evaluated in combination to study how the temporal presence of these three peptides affect osteogenic differentiation. Samples that had only HAVDI or RGDS present from day 0-14 had the same amount of ALP activity as the negative control (hydrogel only). When compared to the positive control (OGP only from day 7-14), samples had higher ALP expression when HAVDI was present from day 0-3 while ALP expression was lower if HAVDI was not present from day 0-3. The presence of RGDS from day 0-3 had a negative impact on ALP expression even when HAVDI was also present. However, the highest ALP activity was seen when only HAVDI was present from day 0-7 and then RGDS and OGP were present from day 7-14. These results strongly indicate that cell-cell interactions play a key role in promoting cell proliferation and tissue morphogenesis at earlier time points, specifically within the first three days, while cell-matrix and osteogenic growth factors are important for cell adhesion and stimulating differentiation at later time points during early osteogenic differentiation.

5.2 Future Work

Further developments and applications for this platform are beyond the scope of this thesis; however, this work provides a baseline for exploring many new areas of interest.

5.2.1 Spatiotemporally Controlling RGDS, HAVDI and OGP

Building from the work completed in Chapter 4, the next steps would be to add spatial control and form gradients on the hydrogel surface. This would allow the user to evaluate how changes in RGDS and HAVDI concentration along with their temporal presentation effect osteogenesis using a single platform. Vega et al. have used NorHA hydrogels to form RGDS and HAVDI gradients to study their effect on chondrogenesis using a high-throughput screening technique.[19] This approach could be applied to the NorHA-DNA platform to assess gene expression of collagen I (proliferative stage), ALP (matrix maturation stage), and osteocalcin (mineralization stage). These three genes would provide insight into the role of cell-cell (via HAVDI) and cell-matrix (via RGDS) interactions during the three stages of osteogenesis.[83–85] Another important study would use a metabolic assay (e.g. bromodeoxyuridine incorporation) to study cell proliferation in response to the spatiotemporal presentation of RGDS and HAVDI.

5.2.2 Bone Morphogenetic Protein Binding via GAG-Mimetic Polymers

Another advancement from the work completed in Chapter 4 would be to switch from using peptides to full length proteins, specifically bone morphogenetic proteins

(BMPs). BMPs have been shown to be a promising therapeutic for supporting bone regeneration, where BMP-2 and BMP-7 are FDA-approved.[117,118] However, supraphysiological concentrations are required for adequate osteoinduction due to poor spatiotemporal control.[119–122] Tethering BMPs to DNA has been shown to be very wasteful and reduce protein activity.[123] One approach is to use glycosaminoglycan (GAG)-mimetic polymers that will bind to BMP. Biotin incorporated into the polymer will allow the user to attach the polymer to biotin-DNA via streptavidin addition. Displacement DNA strands will remove the biotin-DNA along with the polymer and any adhered BMPs from the surface. By combining BMPs with the NorHA-DNA platform, this could enable improved growth factor efficacy and increase osteoinduction.

5.2.3 Coiled-Coil Peptides for In Vivo Applications

Since DNA is present in all living systems, the use of DNA as a linker restricts the application of this platform to *in vitro* models; however, switching from DNA to coiled-coil peptides as linkers would allow this system to be used *in vivo*. Coiled-coils are bundles of amphipathic helices and have been used as peptide-based linkers.[124–127] One major advantage to coiled-coils is that they can be genetically fused to proteins which would greatly simplify the incorporation of bioactive proteins with spatiotemporal control. Synthesizing coiled-coils peptides conjugated with biomolecules of interest would limit the amount of synthesis steps required to reach the final product. This would increase biomolecule yield which would enable the use of higher concentrations on the biomaterial surface, which may be necessary for certain biomolecules. There are also many pairs of coiled-coils that exist allowing for orthogonal control of two or more

signals similar to DNA. The coiled-coil system can be designed to be reversible by altering the number of helices on each coiled-coil strand.[128,129] For example, a short coil with three helices can be tethered to the biomaterial surface while a longer coil, that has the biomolecule of interest, with four helices can bind to the short coil with an overhang ending. To remove the biomolecule, a displacement coil that has four helices can be introduced which will bind to the overhang region on the peptide coil and outcompete the short strand.

5.2.4 Spatiotemporally Controlling Biomolecules on Electrospun Fibers

Lastly, this approach could be used to create a pseudo 3D environment by incorporating DNA onto electrospun fibers. The combination of electrospinning with reversible DNA handles would enable the creation of fiber alignment gradients with spatiotemporally controlled chemical gradients. The development of such a platform could be used to study how cell behavior changes in response to both chemical and physical stimuli. One area of application is to mimic the tendon-bone junction. The physical structure of tendon is highly fibrous and aligned[130,131] while bone is highly mineralized.[78,132] The transition from highly aligned fibers to mineralized tissue occurs gradually. Peptide gradients can be used to mimic this biochemical transition and preferentially promote tenogenesis and osteogenesis in the correct locations. Overall, the HA-DNA platform developed in this dissertation can be altered to better mimic the natural environment of a wide range of tissue types.

REFERENCES

1. Fumasi, F. M., Stephanopoulos, N. & Holloway, J. L. Reversible control of biomaterial properties for dynamically tuning cell behavior. *J. Appl. Polym. Sci.* **137**, 49058 (2020).

2. Gattazzo, F., Urciuolo, A. & Bonaldo, P. Extracellular matrix: A dynamic microenvironment for stem cell niche. *Biochimica et Biophysica Acta - General Subjects* vol. 1840 2506–2519 (2014).

3. Rozario, T. & DeSimone, D. W. The extracellular matrix in development and morphogenesis: A dynamic view. *Developmental Biology* vol. 341 126–140 (2010).

4. Lu, P., Weaver, V. M. & Werb, Z. The extracellular matrix: A dynamic niche in cancer progression. *Journal of Cell Biology* vol. 196 395–406 (2012).

5. Gerstenfeld, L. C., Cullinane, D. M., Barnes, G. L., Graves, D. T. & Einhorn, T. A. Fracture healing as a post-natal developmental process: Molecular, spatial, and temporal aspects of its regulation. *J. Cell. Biochem.* **88**, 873–884 (2003).

6. Velnar, T., Bailey, T. & Smrkolj, V. The wound healing process: An overview of the cellular and molecular mechanisms. *Journal of International Medical Research* vol. 37 1528–1542 (2009).

7. Dimitriou, R., Tsiridis, E. & Giannoudis, P. V. Current concepts of molecular aspects of bone healing. *Injury* (2005) doi:10.1016/j.injury.2005.07.019.

8. Marsell, R. & Einhorn, T. A. The biology of fracture healing. *Injury* **42**, 551–555 (2011).

9. Velnar, T., Bailey, T. & Smrkolj, V. *The Wound Healing Process: an Overview of the Cellular and Molecular Mechanisms. The Journal of International Medical Research* vol. 37 (2009).

10. Ulery, B. D., Nair, L. S. & Laurencin, C. T. Biomedical applications of

biodegradable polymers. *Journal of Polymer Science, Part B: Polymer Physics* vol. 49 832–864 (2011).

11. Seliktar, D. Designing cell-compatible hydrogels for biomedical applications. *Science* vol. 336 1124–1128 (2012).

12. Murphy, W. L., McDevitt, T. C. & Engler, A. J. Materials as stem cell regulators. *Nat. Mater.* **13**, 547–557 (2014).

13. Jung, Y. L. & Donahue, H. J. Cell sensing and response to micro- and nanostructured surfaces produced by chemical and topographic patterning. *Tissue Engineering* vol. 13 1879–1891 (2007).

14. Bettinger, C. J., Langer, R. & Borenstein, J. T. Engineering substrate topography at the Micro- and nanoscale to control cell function. *Angewandte Chemie - International Edition* vol. 48 5406–5415 (2009).

15. Keselowsky, B. G., Collard, D. M. & García, A. J. Surface chemistry modulates fibronectin conformation and directs integrin binding and specificity to control cell adhesion. *J. Biomed. Mater. Res. - Part A* **66**, 247–259 (2003).

16. Hahn, M. S. *et al.* Photolithographic patterning of polyethylene glycol hydrogels. *Biomaterials* **27**, 2519–2524 (2006).

17. Ker, E. D. F. *et al.* Engineering spatial control of multiple differentiation fates within a stem cell population. *Biomaterials* **32**, 3413–3422 (2011).

18. Wheeldon, I., Farhadi, A., Bick, A. G., Jabbari, E. & Khademhosseini, A. Nanoscale tissue engineering: Spatial control over cell-materials interactions. *Nanotechnology* vol. 22 (2011).

19. Vega, S. L. *et al.* Combinatorial hydrogels with biochemical gradients for screening 3D cellular microenvironments. *Nat. Commun.* **9**, 614 (2018).

20. Gramlich, W. M., Kim, I. L. & Burdick, J. A. Synthesis and orthogonal photopatterning of hyaluronic acid hydrogels with thiol-norbornene chemistry. *Biomaterials* **34**, 9803–9811 (2013).

21. Wade, R. J., Bassin, E. J., Gramlich, W. M. & Burdick, J. A. Nanofibrous hydrogels with spatially patterned biochemical signals to control cell behavior. *Adv. Mater.* **27**, 1356–1362 (2015).

22. Lee, T. T. *et al.* Light-triggered in vivo activation of adhesive peptides regulates cell adhesion, inflammation and vascularization of biomaterials. *Nat. Mater.* **14**, 352–360 (2015).

23. Goubko, C. A. *et al.* Comparative analysis of photocaged RGDS peptides for cell patterning. *J. Biomed. Mater. Res. Part A* **101A**, 787–796 (2013).

24. Wirkner, M. *et al.* Photoactivatable Caged Cyclic RGD Peptide for Triggering Integrin Binding and Cell Adhesion to Surfaces. *ChemBioChem* **12**, 2623–2629 (2011).

25. He, J. *et al.* Microfiber-reinforced nanofibrous scaffolds with structural and material gradients to mimic ligament-to-bone interface †. *J. Mater. Chem. B* **5**, 8579 (2017).

26. Kishan, A. P. *et al.* Fabrication of macromolecular gradients in aligned fiber scaffolds using a combination of in-line blending and air-gap electrospinning. *Acta Biomater.* **56**, 118–128 (2017).

27. Ladd, M. R., Lee, S. J., Stitzel, J. D., Atala, A. & Yoo, J. J. Co-electrospun dual scaffolding system with potential for muscle-tendon junction tissue engineering. *Biomaterials* **32**, 1549–1559 (2011).

28. Patel, N. *et al.* Spatially controlled cell engineering on biodegradable polymer surfaces. *FASEB J.* **12**, 1447–1454 (1998).

29. Kim, D. & Herr, A. E. Protein immobilization techniques for microfluidic assays. *Biomicrofluidics* **7**, (2013).

30. Phillippi, J. A. *et al.* Microenvironments Engineered by Inkjet Bioprinting Spatially Direct Adult Stem Cells Toward Muscle- and Bone-Like Subpopulations. *Stem Cells* **26**, 127–134 (2008).

31. Luo, Y., Wei, X. & Huang, P. 3D bioprinting of hydrogel-based biomimetic microenvironments. *J. Biomed. Mater. Res. Part B Appl. Biomater.* **107**, 1695–1705 (2019).

32. Miller, E. D. *et al.* Spatially directed guidance of stem cell population migration by immobilized patterns of growth factors. *Biomaterials* **32**, 2775–2785 (2011).

33. Auernheimer, J., Dahmen, C., Hersel, U., Bausch, A. & Kessler, H. Photoswitched cell adhesion on surfaces with RGD peptides. *J. Am. Chem. Soc.* **127**, 16107–16110 (2005).

34. Lamb, B. M. & Yousaf, M. N. Redox-switchable surface for controlling peptide structure. *J. Am. Chem. Soc.* **133**, 8870–8873 (2011).

35. Boekhoven, J., Rubertpérez, C. M., Sur, S., Worthy, A. & Stupp, S. I. Dynamic display of bioactivity through host-guest chemistry. *Angew. Chemie - Int. Ed.* **52**, 12077–12080 (2013).

36. Freeman, R. *et al.* Instructing cells with programmable peptide DNA hybrids. *Nat. Commun.* **8**, 1–11 (2017).

37. Hahn, M. S., Miller, J. S. & West, J. L. Three-dimensional biochemical and biomechanical patterning of hydrogels for guiding cell behavior. *Adv. Mater.* **18**, 2679–2684 (2006).

38. Luo, Y. & Shoichet, M. S. A photolabile hydrogel for guided three-dimensional cell growth and migration. *Nat. Mater.* **3**, 249–254 (2004).

39. P, M.-Z. & MS, S. Anisotropic Three-Dimensional Peptide Channels Guide Neurite Outgrowth Within a Biodegradable Hydrogel Matrix. *Biomed. Mater.* **1**, (2006).

40. Mosiewicz, K. A. *et al.* In situ cell manipulation through enzymatic hydrogel photopatterning. *Nat. Mater.* **12**, 1072–1078 (2013).

41. DeForest, C. A. & Anseth, K. S. Cytocompatible click-based hydrogels with dynamically tunable properties through orthogonal photoconjugation and photocleavage reactions. *Nat. Chem.* **3**, 925–931 (2011).

42. DeForest, C. A. & Anseth, K. S. Photoreversible patterning of biomolecules within click-based hydrogels. *Angew. Chemie - Int. Ed.* **51**, 1816–1819 (2012).

43. Deforest, C. A. & Tirrell, D. A. A photoreversible protein-patterning approach for guiding stem cell fate in three-dimensional gels. *Nat. Mater.* **14**, 523–531 (2015).

44. Shadish, J. A., Benuska, G. M. & DeForest, C. A. Bioactive site-specifically modified proteins for 4D patterning of gel biomaterials. *Nat. Mater.* **18**, 1005–1014 (2019).

45. Gandavarapu, N. R., Azagarsamy, M. A. & Anseth, K. S. Photo-click living strategy for controlled, reversible exchange of biochemical ligands. *Adv. Mater.* **26**, 2521–2526 (2014).

46. Grim, J. C. *et al.* A Reversible and Repeatable Thiol-Ene Bioconjugation for Dynamic Patterning of Signaling Proteins in Hydrogels. *ACS Cent. Sci.* **4**, 909–916 (2018).

47. Pinheiro, A. V., Han, D., Shih, W. M. & Yan, H. Challenges and opportunities for structural DNA nanotechnology. *Nature Nanotechnology* vol. 6 763–772 (2011).

48. Chidchob, P. & Sleiman, H. F. Recent advances in DNA nanotechnology. *Current Opinion in Chemical Biology* vol. 46 63–70 (2018).

49. Madsen, M. & Gothelf, K. V. Chemistries for DNA Nanotechnology. *Chemical Reviews* (2019) doi:10.1021/acs.chemrev.8b00570.

50. Macculloch, T., Buchberger, A. & Stephanopoulos, N. Emerging applications of peptide-oligonucleotide conjugates: Bioactive scaffolds, self-assembling systems, and hybrid nanomaterials. *Organic and Biomolecular Chemistry* vol. 17 1668–1682 (2019).

51. Stephanopoulos, N. & Freeman, R. DNA-based materials as self-assembling scaffolds for interfacing with cells. in *Self-Assembling Biomaterials: Molecular Design, Characterization and Application in Biology and Medicine* 157–175 (Elsevier, 2018). doi:10.1016/B978-0-08-102015-9.00008-3.

52. Stephanopoulos, N. Peptide−Oligonucleotide Hybrid Molecules for Bioactive Nanomaterials. (2019) doi:10.1021/acs.bioconjchem.9b00259.

53. Zadegan, R. M. & Norton, M. L. Structural DNA Nanotechnology: From Design to Applications. *Int. J. Mol. Sci.* **13**, 7149–7162 (2012).

54. Yurke, B., Turberfield, A. J., Mills, A. P., Simmel, F. C. & Neumann, J. L. A DNA-fuelled molecular machine made of DNA. *Nature* **406**, 605–608 (2000).

55. Dickerson, R. E. *et al.* The anatomy of A-, B-, and Z-DNA. *Science (80-.).* **216**, 475–485 (1982).

56. Endo, M., Hidaka, K., Kato, T., Namba, K. & Sugiyama, H. DNA prism structures constructed by folding of multiple rectangular arms. *J. Am. Chem. Soc.* **131**, 15570–15571 (2009).

57. Ke, Y. *et al.* Scaffolded DNA origami of a DNA tetrahedron molecular container. *Nano Lett.* **9**, 2445–2447 (2009).

58. Kuzuya, A. & Komiyama, M. Design and construction of a box-shaped 3D-DNA origami. *Chem. Commun.* 4182–4184 (2009) doi:10.1039/b907800b.

59. Um, S. H. *et al.* Enzyme-catalysed assembly of DNA hydrogel. *Nat. Mater.* **5**, 797–801 (2006).

60. Xing, Y. *et al.* Self-assembled DNA hydrogels with designable thermal and enzymatic responsiveness. *Adv. Mater.* **23**, 1117–1121 (2011).

61. Blakely, B. L. *et al.* A DNA-based molecular probe for optically reporting cellular traction forces. *Nat. Methods* **11**, 1229–1232 (2014).

62. Wang, X. & Ha, T. Defining single molecular forces required to activate integrin and Notch signaling. *Science (80-.).* **340**, 991–994 (2013).

63. Zhang, Y., Ge, C., Zhu, C. & Salaita, K. DNA-based digital tension probes reveal integrin forces during early cell adhesion. *Nat. Commun.* **5**, (2014).

64. Jiang, F. X., Yurke, B., Schloss, R. S., Firestein, B. L. & Langrana, N. A. The relationship between fibroblast growth and the dynamic stiffnesses of a DNA crosslinked hydrogel. *Biomaterials* **31**, 1199–1212 (2010).

65. Stephanopoulos, N. & Francis, M. B. Choosing an effective protein bioconjugation strategy. *Nature Chemical Biology* vol. 7 876–884 (2011).

66. Marie, P. J. Role of N-Cadherin in bone formation. *J. Cell. Physiol.* **190**, 297–305 (2002).

67. Ferrari, S. L. *et al.* A Role for N-Cadherin in the Development of the Differentiated Osteoblastic Phenotype. *J. Bone Miner. Res.* **15**, 198–208 (2010).

68. Madl, C. M. & Heilshorn, S. C. Engineering Hydrogel Microenvironments to Recapitulate the Stem Cell Niche. (2018) doi:10.1146/annurev-bioeng-062117.

69. Salasznyk, R. M., Williams, W. A., Boskey, A., Batorsky, A. & Plopper, G. E. Adhesion to vitronectin and collagen I promotes osteogenic differentiation of human mesenchymal stem cells. *J. Biomed. Biotechnol.* **2004**, 24–34 (2004).

70. Huang, C.-H., Chen, M.-H., Young, T.-H., Jeng, J.-H. & Chen, Y.-J. Interactive Effects of Mechanical Stretching and Extracellular Matrix Proteins on Initiating

Osteogenic Differentiation of Human Mesenchymal Stem Cells. *J. Cell. Biochem* **108**, 1263–1273 (2009).

71. Schwab, E. H. *et al.* Distinct effects of rgd-glycoproteins on integ-rin-mediated adhesion and osteogenic differentiation of human mesenchymal stem cells. *Int. J. Med. Sci.* **10**, 1846–1859 (2013).

72. Mathews, S., Bhonde, R., Gupta, P. K. & Totey, S. Extracellular matrix protein mediated regulation of the osteoblast differentiation of bone marrow derived human mesenchymal stem cells. *Differentiation* **84**, 185–192 (2012).

73. Zhang, D. Y. & Seelig, G. Dynamic DNA nanotechnology using strand-displacement reactions. *Nat. Chem.* **3**, 103–113 (2011).

74. Lin, D. C., Yurke, B. & Langrana, N. A. Inducing reversible stiffness changes in DNA-crosslinked gels. *J. Mater. Res.* **20**, 1456–1464 (2005).

75. Buchberger, A. *et al.* Reversible Control of Gelatin Hydrogel Stiffness by Using DNA Crosslinkers** ChemBioChem. *ChemBioChem* **22**, 1755–1760 (2021).

76. Li, N., Wang, H., Qu, X. & Chen, Y. Synthesis of Poly(norbornene-methylamine), a Biomimetic of Chitosan, by Ring-Opening Metathesis Polymerization (ROMP). doi:10.3390/md15070223.

77. Wang, Y., Rapakousiou, A. & Astruc, D. ROMP synthesis of cobalticenium-enamine polyelectrolytes. *Macromolecules* **47**, 3767–3774 (2014).

78. Yang, P. J. & Temenoff, J. S. Engineering orthopedic tissue interfaces. *Tissue Engineering - Part B: Reviews* vol. 15 127–141 (2009).

79. Miserez, A., Schneberk, T., Sun, C., Zok, F. W. & Waite, J. H. The transition from stiff to compliant materials in squid beaks. *Science (80-.).* **319**, 1816–1819 (2008).

80. Sant, S., Hancock, M. J., Donnelly, J. P., Iyer, D. & Khademhosseini, A.

Biomimetic gradient hydrogels for tissue engineering. *Can. J. Chem. Eng.* **88**, 899–911 (2010).

81. Huang, Z., Nelson, E. R., Smith, R. L. & Goodman, S. B. The Sequential Expression Profiles of Growth Factors from Osteroprogenitors to Osteoblasts In Vitro. *https://home.liebertpub.com/ten* **13**, 2311–2320 (2007).

82. Birmingham, A. & McNamara, L. M. Title Osteogenic differentiation of mesenchymal stem cells is regulated by osteocyte and osteoblast cells in a simplified bone niche. *Eur. Cells Mater.* **23**, 13–27.

83. Kim, E. J. *et al.* Post microtextures accelerate cell proliferation and osteogenesis. *Acta Biomater.* **6**, 160–169 (2010).

84. Robert, A. W., Marcon, B. H., Dallagiovanna, B. & Shigunov, P. Adipogenesis, Osteogenesis, and Chondrogenesis of Human Mesenchymal Stem/Stromal Cells: A Comparative Transcriptome Approach. *Front. Cell Dev. Biol.* **8**, (2020).

85. Infante, A. & Rodríguez, C. I. Osteogenesis and aging: lessons from mesenchymal stem cells. *Stem Cell Res. Ther. 2018 91* **9**, 1–7 (2018).

86. Marie, P. J., Haÿ, E. & Saidak, Z. Integrin and cadherin signaling in bone: Role and potential therapeutic targets. *Trends in Endocrinology and Metabolism* vol. 25 567–575 (2014).

87. Marie, P. J. *et al.* Cadherin-mediated cell-cell adhesion and signaling in the skeleton. *Calcified Tissue International* vol. 94 46–54 (2014).

88. Marie, P. J. & Haÿ, E. Cadherins and Wnt signalling: a functional link controlling bone formation. *Bonekey Rep.* **2**, (2013).

89. Marie, P. J. & Teti, A. Integrins and other cell surface attachment molecules of bone cells. in *Principles of Bone Biology* 401–422 (Elsevier, 2019). doi:10.1016/B978-0-12-814841-9.00017-8.

90. Bicho, D., Ajami, S., Liu, C., Reis, R. L. & Oliveira, J. M. Peptide-biofunctionalization of biomaterials for osteochondral tissue regeneration in early stage osteoarthritis: Challenges and opportunities. *Journal of Materials Chemistry B* vol. 7 1027–1044 (2019).

91. Kechagia, J. Z., Ivaska, J. & Roca-Cusachs, P. Integrins as biomechanical sensors of the microenvironment. *Nature Reviews Molecular Cell Biology* vol. 20 457–473 (2019).

92. Anderson, L. R., Owens, T. W. & Naylor, M. J. Structural and mechanical functions of integrins. *Biophysical Reviews* vol. 6 203–213 (2014).

93. Bachmann, M., Kukkurainen, S., Hytönen, V. P. & Wehrle-Haller, B. Cell adhesion by integrins. *Physiol. Rev.* **99**, 1655–1699 (2019).

94. Alimperti, S. & Andreadis, S. T. CDH2 and CDH11 act as regulators of stem cell fate decisions. *Stem Cell Research* vol. 14 270–282 (2015).

95. Maître, J. L. & Heisenberg, C. P. Three functions of cadherins in cell adhesion. *Current Biology* vol. 23 (2013).

96. Schultz, G. S. & Wysocki, A. Interactions between extracellular matrix and growth factors in wound healing. *Wound Repair and Regeneration* vol. 17 153–162 (2009).

97. Wilgus, T. A. Growth Factor–Extracellular Matrix Interactions Regulate Wound Repair. *Adv. Wound Care* **1**, 249–254 (2012).

98. Briquez, P. S., Hubbell, J. A. & Martino, M. M. Extracellular Matrix-Inspired Growth Factor Delivery Systems for Skin Wound Healing. *Adv. Wound Care* **4**, 479–489 (2015).

99. Lee, K., Silva, E. A. & Mooney, D. J. Growth factor delivery-based tissue engineering: General approaches and a review of recent developments. *Journal of the Royal Society Interface* vol. 8 153–170 (2011).

100. Pigossi, S. C., Medeiros, M. C., Saska, S., Cirelli, J. A. & Scarel-Caminaga, R. M. Role of osteogenic growth peptide (OGP) and OGP(10–14) in bone regeneration: A review. *International Journal of Molecular Sciences* vol. 17 (2016).

101. Bab, I. & Chorev, M. Osteogenic growth peptide: From concept to drug design. *Biopolymers - Peptide Science Section* vol. 66 33–48 (2002).

102. Policastro, G. M. & Becker, M. L. Osteogenic growth peptide and its use as a bio-conjugate in regenerative medicine applications. *Wiley Interdiscip. Rev. Nanomedicine Nanobiotechnology* **8**, 449–464 (2016).

103. Kim, I. L., Khetan, S., Baker, B. M., Chen, C. S. & Burdick, J. A. Fibrous hyaluronic acid hydrogels that direct MSC chondrogenesis through mechanical and adhesive cues. *Biomaterials* **34**, 5571–5580 (2013).

104. Marklein, R. A. & Burdick, J. A. Spatially controlled hydrogel mechanics to modulate stem cell interactions. *Soft Matter* **6**, 136–143 (2009).

105. Engler, A. J., Sen, S., Sweeney, H. L. & Discher, D. E. Matrix Elasticity Directs Stem Cell Lineage Specification. *Cell* **126**, 677–689 (2006).

106. Wen, J. H. *et al.* Interplay of matrix stiffness and protein tethering in stem cell differentiation. *Nat. Mater.* **13**, 979–987 (2014).

107. Eroshenko, N., Ramachandran, R., Yadavalli, V. K. & Rao, R. R. Effect of substrate stiffness on early human embryonic stem cell differentiation. *J. Biol. Eng.* **7**, 1–8 (2013).

108. Mao, A. S., Shin, J. W. & Mooney, D. J. Effects of substrate stiffness and cell-cell contact on mesenchymal stem cell differentiation. *Biomaterials* **98**, 184–191 (2016).

109. Stains, J. P. & Civitelli, R. Cell-cell interactions in regulating osteogenesis and osteoblast function. *Birth Defects Res. Part C Embryo Today Rev.* **75**, 72–80 (2005).

110. Bellido, T., Plotkin, L. I. & Bruzzaniti, A. Bone Cells. in *Basic and Applied Bone Biology* 27–45 (Elsevier Inc., 2013). doi:10.1016/B978-0-12-416015-6.00002-2.

111. Tian, Y., Cohen, E. D. & Morrisey, E. E. The importance of Wnt signaling in cardiovascular development. in *Pediatric Cardiology* vol. 31 342–348 (NIH Public Access, 2010).

112. Reya, T. *et al.* Wnt signaling regulates B lymphocyte proliferation through a LEF-1 dependent mechanism. *Immunity* **13**, 15–24 (2000).

113. Cohen, E. D. *et al.* Wnt/β-catenin signaling promotes expansion of Isl-1-positive cardiac progenitor cells through regulation of FGF signaling. *J. Clin. Invest.* **117**, 1794–1804 (2007).

114. Bradley, R. S. & Brown, A. M. A soluble form of Wnt-1 protein with mitogenic activity on mammary epithelial cells. *Mol. Cell. Biol.* **15**, 4616–4622 (1995).

115. Baker, J. C., Beddington, R. S. P. & Harland, R. M. Wnt signaling in Xenopus embryos inhibits Bmp4 expression and activates neural development. *Genes Dev.* **13**, 3149–3159 (1999).

116. Goessling, W. *et al.* Genetic Interaction of PGE2 and Wnt Signaling Regulates Developmental Specification of Stem Cells and Regeneration. *Cell* **136**, 1136–1147 (2009).

117. Seeherman, H. & Wozney, J. M. Delivery of bone morphogenetic proteins for orthopedic tissue regeneration. *Cytokine Growth Factor Rev.* **16**, 329–345 (2005).

118. Boden, S. D., Kang, J., Sandhu, H. & Heller, J. G. Use of recombinant human bone morphogenetic protein-2 to achieve posterolateral lumbar spine fusion in humans: A prospective, randomized clinical pilot trial 2002 volvo award in clinical studies. *Spine (Phila. Pa. 1976).* **27**, 2662–2673 (2002).

119. Stevens, M. M. Biomaterials for bone tissue engineering. *Mater. Today* **11**, 18–25 (2008).

120. Meijer, G. J., Bruijn, J. D. de, Koole, R. & Blitterswijk, C. A. van. Cell-Based Bone Tissue Engineering. *PLoS Med.* **4**, 0260–0264 (2007).

121. Mehta, M., Schmidt-Bleek, K., Duda, G. N. & Mooney, D. J. Biomaterial delivery of morphogens to mimic the natural healing cascade in bone. *Adv. Drug Deliv. Rev.* **64**, 1257–1276 (2012).

122. Tannoury, C. A. & An, H. S. Complications with the use of bone morphogenetic protein 2 (BMP-2) in spine surgery. *Spine J.* **14**, 552–559 (2014).

123. Erkelenz, M., Kuo, C.-H. & Niemeyer, C. M. DNA-Mediated Assembly of Cytochrome P450 BM3 Subdomains. *J. Am. Chem. Soc.* **133**, 16111–16118 (2011).

124. Maxim G. Ryadnov, †, Buelent Ceyhan, ‡, Christof M. Niemeyer, *,‡ and & Derek N. Woolfson*, †. "Belt and Braces": A Peptide-Based Linker System of de Novo Design. *J. Am. Chem. Soc.* **125**, 9388–9394 (2003).

125. Grewal, M. G., Gray, V. P., Letteri, R. A. & Highley, C. B. User-defined, temporal presentation of bioactive molecules on hydrogel substrates using supramolecular coiled coil complexes †. *Cite this Biomater. Sci* **9**, 4374 (2021).

126. Mason, J. M. & Arndt, K. M. Coiled Coil Domains: Stability, Specificity, and Biological Implications. *ChemBioChem* **5**, 170–176 (2004).

127. Truebestein, L. & Leonard, T. A. Coiled-coils: The long and short of it. *Bioessays* **38**, 903 (2016).

128. Gröger, K., Gavins, G. & Seitz, O. Strand Displacement in Coiled-Coil Structures: Controlled Induction and Reversal of Proximity. *Angew. Chemie Int. Ed.* **56**, 14217–14221 (2017).

129. Riker, K. D. *et al.* A Programmable Toolkit to Dynamically Signal Cells Using Peptide Strand Displacement. *ACS Appl. Mater. Interfaces* **13**, 21018–21029 (2021).

130. Gillies, A. R. & Lieber, R. L. Structure and Function of the Skeletal Muscle Extracellular Matrix. *Muscle Nerve* **44**, 318 (2011).

131. Provenzano, P. P. & Vanderby, R. Collagen fibril morphology and organization: Implications for force transmission in ligament and tendon. *Matrix Biol.* **25**, 71–84 (2006).

132. Apostolakos, J. *et al.* The enthesis: a review of the tendon-to-bone insertion. *Muscles. Ligaments Tendons J.* **4**, 333 (2014).